



A REFINEMENT AND CROSS-VALIDATION OF
THE SPECIAL SENSOR MICROWAVE IMAGER
(SSM/I) CALIBRATION-VALIDATION (CV)
BRIGHTNESS TEMPERATURE ALGORITHM

THESIS

Mark R. Adair, Captain, USAF
AFIT/GM/ENP/99M-01

19990402 023

DEPARTMENT OF THE AIR FORCE
AIR UNIVERSITY
AIR FORCE INSTITUTE OF TECHNOLOGY

Wright-Patterson Air Force Base, Ohio

APPROVED FOR PUBLIC RELEASE; DISTRIBUTION UNLIMITED



DTIC QUALITY INSPECTED 2

A REFINEMENT AND CROSS-VALIDATION OF
THE SPECIAL SENSOR MICROWAVE IMAGER
(SSM/I) CALIBRATION-VALIDATION (CV)
BRIGHTNESS TEMPERATURE ALGORITHM

THESIS

Mark R. Adair, Captain, USAF
AFIT/GM/ENP/99M-01

DEPARTMENT OF THE AIR FORCE
AIR UNIVERSITY
AIR FORCE INSTITUTE OF TECHNOLOGY

Wright-Patterson Air Force Base, Ohio

APPROVED FOR PUBLIC RELEASE; DISTRIBUTION UNLIMITED

The views expressed in this thesis are those of the author, and do not reflect the official policy or position of the Department of Defense, or the U.S. Government.

**A Refinement and Cross-Validation of the
Special Sensor Microwave Imager (SSM/I)
Calibration-Validation (CV) Brightness Temperature
Algorithm**

THESIS

Presented to the faculty of the
Graduate School of Engineering
of the Air Force Institute of Technology
Air University

In Partial Fulfillment of the
Requirements for the Degree of
Master of Science (Meteorology)

Mark R. Adair, B.A., B.S.

Captain, USAF

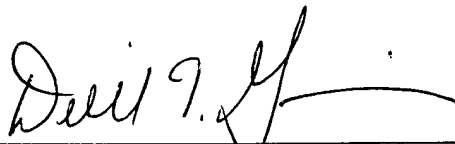
March, 1999

A REFINEMENT AND CROSS-VALIDATION OF THE SPECIAL SENSOR
MICROWAVE IMAGER (SSM/I) CALIBRATION-VALIDATION (CV)
BRIGHTNESS TEMPERATURE ALGORITHM

Mark Richard Adair, B.A., B.S.

Captain, United States Air Force

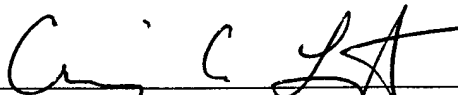
Approved:



Derrill T. Goldizen, Maj, USAF
Chairman, Advisory Committee

24 Feb 99

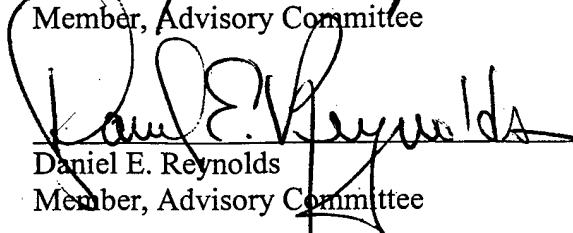
Date



Craig C. Largent, Capt, USAF
Member, Advisory Committee

22 Feb 99

Date



Daniel E. Reynolds
Member, Advisory Committee

Feb 22, 1999

Date

Acknowledgments

First, I would like to thank Major Derrill Goldizen, my thesis advisor. He was always ready with advice and made sure my research did not stray too far off course. Dan Reynolds, extraordinary statistician and thesis committee member, always made time for my statistical questions and conundrums. Captain Craig Largent, whose office was happily next door to Major Goldizen's, was always ready to pipe up with constructive input to discussions he overheard from next door. My sponsor at Air Force Weather Agency, Major Mike Farrar, has my gratitude for taking time from his busy schedule to give my thesis a thorough peer review-style examination.

I would also like to express my appreciation to those who helped me acquire and decode data. Captain Charles Harris and Captain Ron Comoglio were always eager to explain their research and help me get on track with mine. Lt Col Mike Walters was very helpful with FORTRAN questions. For their assistance in my data acquisition efforts, I would like to thank MSgt Pete Rahe here at AFIT, MSgt Glenn Harris from AFCCC, SSgt Chris Wade from AFWA, and Mr. Sushma Gupta from NGDC. Thanks also to Capt Dave Coxwell of 55th Space Weather Squadron for his valuable input.

Finally, I deeply appreciate the moral support I received from friends and family. Thanks to my parents for listening to the incomprehensible details of my research. Thanks also for the frequent long-distance support from my friends Traci Hilbert, Brad Green, Warren Madden, Laurent Fehlen, Axel Heilmann, and Andrea Wein.

Mark R. Adair

Table of Contents

<i>Acknowledgments</i>	<i>iii</i>
<i>List of Figures</i>	<i>vii</i>
<i>List of Tables</i>	<i>x</i>
<i>Abstract</i>	<i>xi</i>
I. Introduction	1
Chapter Overview	1
Introduction	1
Background	2
Problem and Assumptions	3
Research Scope and General Approach	4
Results	5
Summary	7
II. Background	8
Chapter Overview	8
Introduction	8
Radiative Transfer	10
The Rayleigh-Jeans Approximation	12
Non-Blackbody and Atmospheric Effects	14
Historical Context	16

Table of Contents

DMSP and the SSM/I.....	18
The Inverse Problem.....	21
The General Linear Model.....	23
Stepwise Linear Regression.....	25
Antenna Temperature vs. Brightness Temperature.....	26
The Calibration-Validation (CV) Algorithm.....	26
Indicator Variables and Qualitative Regression.....	27
Sources of Error.....	28
Related Research.....	31
Summary.....	35
III. Methodology.....	36
Chapter Overview.....	36
Past Work at AFIT.....	37
Data Description.....	38
Decoding, Combining, Matching, and Sorting the Data.....	40
Statistics Used.....	45
Summary.....	53
IV. Results Analysis.....	54
Chapter Overview.....	54

Table of Contents

Data Sets.....	54
Qualitative Regression Results.....	54
Discussion.....	55
Regression Coefficient Refinement.....	56
Cross-Validation of the Data Sets.....	61
Summary.....	70
V. Summary, Conclusions and Recommendations.....	71
Summary.....	71
Conclusion and Recommendation for AFWA.....	72
Recommendations for Further Research.....	72
Appendix A: Other Regression Performed but Not Directly Used in the Research.....	75
Appendix B: Residual and Normality Plots of the F10/F13/F14 Regression.....	79
Appendix C: Land Type Algorithms.....	84
Bibliography.....	86
Vita.....	89

List of Figures

1. Planck Radiance by Temperature and Wavelength.....	9
2. Schematic of a DMSP Satellite.....	19
3. SSM/I Scan Geometry.....	20
4. Percentage Transmission through Clear Atmosphere to Space.....	21
5. Polar Stereographic Northern Hemisphere Grid.....	39
6. Methodology Flow Chart.....	41
7. “Superneph” grid over Malmstrom AFB, MT.....	43
8. F Distribution with 7 and 92 Degrees of Freedom, Fcrit shown.....	50
9. F Distribution with 7 and 92 Degrees of Freedom, P-Value shown.....	51
10. Critical Values of t distribution.....	52
11. Scatter Plot for Dry Soil Land Type.....	58
12. Scatter Plot for Moist Soil Land Type.....	58
13. Scatter Plot for Desert Land Type.....	59
14. Scatter Plot for Dense Vegetation Land Type.....	59
15. Scatter Plot for Light Vegetation Land Type.....	60
16. Cross-Validation of F10/F13 Coefficients on F14 Data – Dry Soil.....	62
17. Cross-Validation of F10/F13 Coefficients on F14 Data – Moist Soil.....	62
18. Cross-Validation of F10/F13 Coefficients on F14 Data – Desert.....	63
19. Cross-Validation of F10/F13 Coefficients on F14 Data – Light Vegetation.....	63
20. Cross-Validation of F10/F13 Coefficients on F14 Data – Semidesert.....	64
21. Cross-Validation of F10/F13 Coefficients on F14 Data – Wet Soil.....	64

List of Figures

22. Cross-Validation of F14 Coefficients on F10/F13 Data – Dry Soil.....	65
23. Cross-Validation of F14 Coefficients on F10/F13 Data – Moist Soil.....	65
24. Cross-Validation of F14 Coefficients on F10/F13 Data – Desert.....	66
25. Cross-Validation of F14 Coefficients on F10/F13 Data – Dense Vegetation.....	66
26. Cross-Validation of F14 Coefficients on F10/F13 Data – Light Vegetation.....	67
27. Cross-Validation of F14 Coefficients on F10/F13 Data – Semidesert.....	67
28. Cross-Validation of F14 Coefficients on F10/F13 Data – Wet Soil.....	68
A1. Scatter Plot for Dry Soil Land Type, Jan-Feb 1997, F10/F13.....	75
A2. Scatter Plot for Moist Soil Land Type, Jan-Feb 1997, F10/F13.....	75
A3. Scatter Plot for Semidesert Land Type, Jan-Feb 1997, F10/F13.....	76
A4. Scatter Plot for Desert Land Type, Jan-Feb 1997, F10/F13.....	76
A5. Scatter Plot for Light Vegetation Land Type, Jan-Feb 1997, F10/F13.....	77
A6. Scatter Plot for Wet Soil Land Type, Jan-Feb 1997, F10/F13.....	77
A7. Scatter Plot for Indeterminate Land Type, Jan-Feb 1997, F10/F13.....	78
B1. Residual Plot for Dry Soil Land Type.....	79
B2. Normality Plot for Dry Soil Land Type.....	79
B3. Residual Plot for Moist Soil Land Type.....	80
B4. Normality Plot for Moist Soil Land Type.....	80
B5. Residual Plot for Desert Land Type.....	81
B6. Normality Plot for Desert Land Type.....	81
B7. Residual Plot for Dense Vegetation Land Type.....	82

List of Figures

B8. Normality Plot for Dense Vegetation Land Type..... 82

B9. Residual Plot for Light Vegetation Land Type..... 83

B10. Normality Plot for Light Vegetation Land Type..... 83

List of Tables

1. Data Matches Used in Research.....	38
2. Satellite Data File Names.....	39
3. Example of Data Format.....	40
4. Results of Qualitative Regression.....	55
5. Combined Regression Results (All Satellites, F10/F13/F14).....	60
6. RMSE (K) Comparison to Original CV Regression.....	61
7. RMSE and MSPR Values of F10/F13 Coefficients Cross-Validated on F14 Data.....	68
8. RMSE and MSPR Values of F14 Coefficients Cross-Validated on F10/F13 Data.....	68
9. RMSE (K) of CV Algorithm from Harris (1998).....	69
A1. Regression Results (F10/F13) for Jan-Feb 1997.....	78

Abstract

The Air Force Weather Agency (AFWA) currently uses an algorithm to calculate surface temperatures from microwave observations taken by the Special Sensor Microwave Imager (SSM/I) aboard the orbiting platforms of the Defense Meteorological Satellite Program (DMSP). This algorithm, called the Calibration-Validation (CV) algorithm, uses multiple linear regression to calculate coefficients relating microwave brightness temperatures and land surface temperatures. Because the coefficients in this algorithm do not take into account the identity of the individual satellite, the question arose whether this assumption was valid.

This thesis used multiple linear regression, stepwise linear regression, and qualitative regression on 3700 data sets from October of 1996 and September of 1997, including microwave brightness temperatures from three satellites. This data was analyzed to determine if satellite identity had a significant impact on CV regression coefficients. Analysis indicated that satellite identity does not have a significant impact on regression coefficients for five of the eight CV land types investigated. Analysis of two CV land types indicated data set identity had a significant impact, while there was insufficient data to determine the impact for one CV land type.

In addition to the qualitative regression, stepwise linear regression was performed on five land type categories using combined data for all satellites. Regressed RMSEs ranged from 2.825 K to 3.743 K, while R squared values ranged from .7295 to .8613. Preliminary analysis indicated refinement of CV brightness temperature coefficients might yield better accuracy for the algorithm.

**A REFINEMENT AND CROSS-VALIDATION OF
THE SPECIAL SENSOR MICROWAVE IMAGER (SSM/I)
CALIBRATION/VALIDATION (CV) BRIGHTNESS
TEMPERATURE ALGORITHM**

I. Introduction

Chapter Overview

This chapter introduces satellite passive microwave remote sensing, its use in determination of land surface temperatures, and an explanation why improved accuracy would be beneficial in scientific and military applications. A background section will identify the two space platforms used to obtain microwave brightness temperature measurements and the conversion algorithm refined and cross-validated in this study. The research problem, assumptions, and general research approach will be outlined. Finally, the chapter briefly summarizes the results of the research.

Introduction

Until recently, the only method of determining surface temperature at a given location was to place a thermometer there and have a human read it. Obviously, this is not always possible, especially in sparsely populated or data denied areas. With the increased emphasis on numerical weather prediction, it has become important to determine temperatures in the very regions where such in situ temperature measurements are few and far between. If we can measure terrestrial emissions via satellite and develop

an accurate algorithm for calculating surface temperature, it will greatly aid in initializing computer atmospheric models. In addition, military commanders will have better access to information for their Intelligence Preparation of the Battlefield (IPB) assessments, for example allowing for more accurate weapons lock-on range estimates by such temperature-dependent computer programs as the Electro-optical Tactical Decision Aid (EOTDA). One attempt to measure temperatures via remote sensing is the Calibration/Validation (CV) Algorithm, adapted to the Special Sensor Microwave Imager (SSM/I) aboard the F13 Defense Meteorological Satellite Program (DMSP) Satellite. If research can be performed to improve the accuracy of the algorithm, as well as to cross-validate the algorithm on other DMSP satellites, the benefits to atmospheric modelers and military commanders will be that much more.

Background

Before we delve into the specifics of the algorithm and the passive microwave imager, we must understand why the microwave spectrum would be the best choice for determining surface temperature. An important criterion is that terrestrial emission measurements not be significantly contaminated by extraterrestrial sources, such as the sun. Thus, our measurements must be obtained within the long (wavelength) end of the electromagnetic spectrum (Rees, 1990). A prima facie choice in this range might be the infrared (IR) spectrum; however, clouds have a high albedo in this range (Rees, 1990), thus making daytime surface measurements difficult where there is cloud cover. The microwave spectrum is the best choice for four reasons: readings are not affected by the sun's illumination; microwave radiation penetrates clouds; microwave radiation

penetrates vegetation; and the nature of microwave radiation allows it to be measured more easily from a spaceborne platform (Ulaby, 1981).

On each of the DMSP platforms, there is an SSM/I. This thesis will concentrate on three satellites carrying this imager – the F13 satellite, the F10 satellite, and the newer F14 satellite; the latter was launched in April 1997 from Vandenberg AFB, California (Cooper, 1997). Research has already been done on land temperature analysis with the F13 satellite (Harris, 1998; and Comoglio, 1997), including a comparison of two different brightness temperature algorithms: The Calibration-Validation (CV) algorithm and the TMPSMI (TS) algorithm. This study will concentrate on improving regression coefficients of the CV algorithm because the CV algorithm has a higher production rate and met Air Force Weather Agency (AFWA) accuracy criteria more often than the TS algorithm (Harris, 1998).

Problem and Assumptions

The focus questions of this research are twofold: first, if regression techniques can fine-tune the CV algorithm's coefficients to yield greater accuracy; and second, if the "true" brightness temperature – surface air temperature regression coefficients derived for one set of passive microwave sensors (F10/F13) are identical to those of other identical sensors (e.g. F14), or is there a statistically significant difference in "true" regression coefficients between the sensors.

This research does not attempt to refine the land type determination part of the CV algorithm; it is assumed the techniques and code used are accurate. Another assumption is that the synoptic observations of surface temperature used in this research

are accurate. Finally, we will assume that all sources of error (explained more in detail in Chapter II) can be reduced to an acceptable level using statistical methods alone.

Research Scope and General Approach

This research will only seek to refine coefficients of the existing CV algorithm and check to see if regressed coefficients can be used interchangeably on brightness temperature measurements from all SSM/I platforms. Thanks to previous research in this field (Harris, 1998; and Comoglio, 1997), there already exists on hand a number of brightness temperature data sets from the F10 and F13 satellites, as well as a large number of surface observations from around the world. The first step was to match F10/F13 brightness temperature measurements obtained at frequencies of 19.3 GHz (horizontal and vertical polarizations), 22.2 GHz (vertical polarization), 37 GHz (horizontal and vertical polarizations), and 85.5 GHz (vertical and horizontal polarizations), with surface observation data by location and time to form data sets. These sets were sorted by season, land type, and region. The matching and sorting was accomplished by adapting FORTRAN code written by Harris and Comoglio and by adapting the land type-sorting algorithm from the CV code. The data was then transferred to a PC and statistical analysis was performed using the commercial software package S Plus 4.5, by MathSoft, Inc, Cambridge, Massachusetts.

After the F10/F13 data was analyzed, Similar F14 SSM/I data was matched with synoptic observation data acquired from the Air Force Combat Climatology Center (AFCCC) and sorted the data sets by CV-determined land type. A Bernoulli indicator variable (Neter et al., 1983) was then assigned to each data point by satellite

identification: a value of 0 was assigned to Harris's F10/F13 data and a value of 1 was assigned to the new F14 data.

Results

Some 4,000 usable F10/F13 matches (what constitutes a "match" is explained in Chapter III) were found and divided into eighteen groups: by seasons (Fall 96 and Winter 97) and by one of eight different land types, plus an "undetermined land type" category. Fourteen of eighteen groups had more than 30 data points, thus allowing us to invoke the Central Limit Theorem (Devore, 1991), and therefore justifying the use of linear regression. Multiple Linear Regression on these groups yielded root mean square errors (RMSE) between 2.55 K and 4.58 K, with explanatory power (R squared) between 0.616 and 0.803. This data compares quite favorably to RMSE values ranging from 5.3 K to 19.4 K in Harris's analysis using the original CV coefficients. The error in the current research was lowest for the Desert land type in Winter 97. The lowest RMSE in the Fall 96 data set was for "Light Vegetation" (RMSE 3.13 K). Highest errors were found in the "Undetermined Land Type" category and "Wet Soil" categories in both seasons. Upon closer analysis, it was determined that the "Wet Soil" land type in Fall 96 had a significantly lower RMSE and higher explanatory power when non-CONUS data points were excluded (4.28 K / 0.625 to 3.41 K / 0.688). The other categories only showed slight changes in RMSE when non-CONUS data points were excluded, though the "Undetermined Land Type" category for Fall 96 showed a considerable increase in explanatory power (0.616 to 0.724).

From the F14 data, 2,581 usable matches were found from September 1997. Since only 474 of these matches came from outside CONUS, the data was not separated by region. These matches were then combined with 1,119 data points from Harris's F10/F13 data from October 1996 and performed a qualitative regression using the Bernoulli indicator variable described earlier. This analysis indicated satellite identity did not have a statistically significant impact upon the regression coefficients for the "Moist Soil," "Dense Vegetation," "Light Vegetation," "Desert," and "Dry, Arable Soil" land types. Satellite identity did have a statistically significant impact upon the regression coefficients for the "Semidesert" and "Wet Soil" land types, as well as for those data sets which the CV algorithm could not confirm a land type. A determination could not be made for the "Mixed Water and Vegetation" land type, as there were no data points in this category.

For the five land types for which satellite identity did not have an impact, new regressions (sans indicator variable) of the combined F10/F13/F14 data sets were performed. RMSEs from the new regression ranged from 2.825 K for the "Light Vegetation" land type to 3.743 K for the "Desert" land type. R squared values ranged from .7295 for "Desert" to .8613 for "Dense Vegetation."

To confirm the qualitative results of the regressions, the F10/F13 and F14 data were regressed separately and each data set was cross-validated using the regressed coefficient from the other data set. Results largely confirmed the qualitative regression, with root MSPR values ranging from 2.687 K for the F14 "Light Vegetation" data validated with the F10/F13 coefficients, to 4.773 K for the F14 "Desert" data validated with the F10/F13 coefficients. Similar validation of the rejected land types confirmed the

rejection, with root MSPR values ranging from 5.22 K for F14 “semidesert” data validated with F10/F13 data, to 7.072 K for F10/F13 “semidesert” data validated with F14 coefficients.

Summary

The purpose of this research is to refine the CV coefficients for improved accuracy in retrieved surface temperature measurements and to determine the compatibility of data from different SSM/I platforms for the purpose of deriving Multiple Linear Regression Coefficients. Multiple Linear Regression analysis was used on Harris’s data to re-derive CV coefficients, reducing the RMSE values by significant amounts over the original CV coefficients. F14 data was then matched, sorted, and combined with Harris’s data. A qualitative regression was then performed to determine if satellite identity was an important factor in the regressions. The research indicated that the platform was not a significant contributor for 5 of the 8 land types. Satellite identity was significant for 2 land types, as well as data points for which the CV algorithm could not determine a land type. There was insufficient data for regression of one of the land types. Cross-validation of the data largely confirmed these results.

II. Background

Chapter Overview

In this chapter, the physics of electromagnetic radiation will be introduced, including Planck's Law and the applicability of the Rayleigh-Jeans Approximation in the microwave region of the spectrum. After the introduction, the history of microwave remote sensing will be discussed briefly. Then, the Defense Meteorological Satellite Program (DMSP) satellites and the SSM/I sensors particular to the study will be discussed. At this point, an equation relating surface temperature to the amount of microwave radiation emitted will be described. It will then be shown that the equation cannot be solved analytically due to the inverse nature of the problem. However, due to large amounts of data available, statistical methods such as multiple linear regression can be used to estimate the actual relationship between the brightness temperatures measured by the satellite and the observed surface temperatures. The Calibration/Validation (CV) algorithm is one such attempt to estimate surface temperatures in such a way. After outlining the advantages of refining CV coefficients and cross-validating algorithms on data from different DMSP satellites, potential sources of error in determining surface temperatures with passive microwave radiometry will be outlined. Finally, a short review of research correlating surface temperatures with microwave emissions will be presented.

Introduction

All objects emit energy in varying intensities throughout the electromagnetic spectrum. The intensity of this emission at a given wavelength is a function of the object's temperature (Rees, 1990). Since we are interested in the temperature of the

earth, we will look at the wavelength distribution of radiation for a body of approximately 300K. If we apply Planck's Law (Fleagle and Businger, 1980) and for the purposes of illustration equate the earth to a black body of 300K and examine the spectrum of its emissions (see Figure 1), we see that the peak of the earth's radiation would fall between 3 and 15 micrometers, the infrared (IR) portion of the spectrum. While viewing the infrared portion allows relatively easy temperature determination, the existence of clouds makes measurement of surface temperatures difficult (although the determination of the temperature of cloud tops can be extremely useful for other meteorological purposes). Because of this, and for the other reasons we discussed earlier, scientists have turned to the microwave portion of the spectrum for surface temperature measurement.

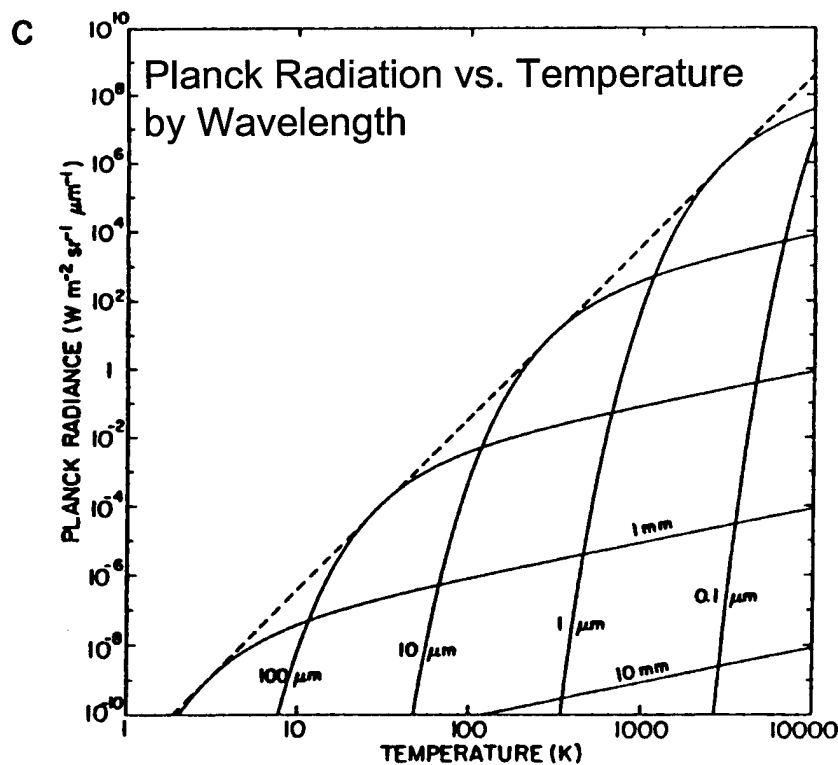


Figure 1: Planck Radiance by Temperature and Wavelength (Adapted from Kidder and Vonder Haar, 1995)

When comparing in situ synoptic surface temperature measurements with temperatures calculated from remotely sensed measurements of terrestrial emission in the microwave portion of the spectrum, there are several potential sources of variance between the two values. One fundamental source of variance arises from the difference in measurement method. In a standard thermometer, the sensor is in direct contact with the air and determines the temperature via conduction, i.e. allowing kinetic energy from the surrounding air molecules to be transferred to the sensor. In contrast, because it is by definition not in direct contact with the earth or its atmosphere, a sensor on board an orbiting platform must be a remote sensor. Also, a satellite-based instrument designed to sense microwave emissions is measuring the magnitude of radiation coming from a particular solid angle of view. As such, a satellite must take into account the shape of the earth and the incident angle of the earth's surface and atmosphere relative to the sensor (Ulaby, 1981).

Radiative Transfer

Radiative transfer is the flow of energy from an object to a receiver at or near the speed of light. While there are equations that quantify this radiation flow, detailed exploration of these equations does not contribute much to the understanding of radiative transfer we need for this research. Therefore, we will keep this discussion as qualitative as possible. Paraphrasing Ulaby (1981), the intensity of radiation measured at a sensor is given by two terms. The first term is the radiation from the object propagating toward the sensor. A negative exponential extinction factor due to absorption by material (or the

“medium”) reduces the magnitude of this first term between the sensor and the object.

The second term represents the emission and scattering by the intervening medium along the propagation path.

Before we proceed, a brief word on polarization. Polarization is the orientation of a wave, in this case electromagnetic waves, relative to a coordinate system (Rees, 1990). In the propagation of an electromagnetic wave, the electric field vector and magnetic intensity vectors are orthogonal (Fleagle and Businger, 1980). As a result, it is important for a sensor to take into account two polarizations of radiation and use vector addition to be able to interpret a full picture of an electromagnetic wave. Finally, due to sign conventions, it is possible that a reading in a given polarization may have a negative contribution to the intensity of the electromagnetic wave. Therefore, we should not be surprised if regression yields oppositely signed coefficients for two polarizations in the same frequency range.

Now that a simplified explanation the physics of radiative transfer has been given, let us simplify the scenario even further: suppose there is no intervening material between object and sensor. This removes the extinction factor from the first term, and the second term altogether, which leaves us with a highly desirable result: brightness temperature measured at the sensor is equal to the brightness temperature (and ultimately, the physical temperature) of the object.

As a final simplification, let us now assume the object is a blackbody, i.e. an idealized, perfectly opaque material that absorbs all radiation at all frequencies, reflecting none, and emits radiation such that its temperature neither increases nor decreases as a result (Ulaby, 1981). At this point, we can now invoke Planck’s radiation law:

$$B_\nu(T) = (2h\nu^3 / c^2)(1/(\exp(h\nu/kT) - 1)) \quad (1)$$

Where B_ν = Surface brightness (or radiance) ($\text{W m}^{-2} \text{sr}^{-1} \text{Hz}^{-1}$)

ν = Frequency (Hz)

T = Physical temperature (K)

h = Planck's Constant ($6.6256 \times 10^{-34} \text{ J s}$)

k = Boltzmann's Constant ($1.3805 \times 10^{-23} \text{ J K}^{-1}$)

c = Speed of light ($2.9979 \times 10^8 \text{ m s}^{-1}$)

B_ν does not have a physical meaning unless the equation is integrated over a range of frequencies. Normally, monochromatic radiance is measured in units of Watts per meter squared per steradian per Hertz, implying integration over the frequency bandwidth of the sensor channel.

After all of our simplifications, we are still left with a rather troublesome equation to evaluate. It would be very nice if we could somehow reduce equation (1) to a polynomial. One way to change an exponential into a polynomial is to convert the exponential into a Taylor polynomial expansion.

The Rayleigh-Jeans Approximation

Even for those of us who are not adept at mathematics, there is a sense of satisfaction when a mathematical technique can be used to simplify a problem. In the case of equation (1), we can expand the exponential using the Taylor expansion:

$$e^x = 1 + x + (x^2 / 2!) + (x^3 / 3!) + \dots \quad (2)$$

In this case, $x = hv/kT$. If we now perform a dimensional analysis of the value of hv/kT in the case of $T \sim 100K$ and frequency in the microwave region (i.e. approximately 100 GHz) we get:

$$h\nu/kT \cong (10^{-34} \cdot 10^{11}) / (10^{-23} \cdot 10^2) \sim 10^{-2} \ll 1 \quad (3)$$

Thus, for the magnitudes in question for this research, we can neglect the higher order terms of hv/kT , leaving us with the approximation $e^x = 1 - x$. This gives us when we plug back into equation (1):

$$B_\nu(T) = (2h\nu^3 / c^2) (1 / ((1 - h\nu/kT) - 1)) = 2h\nu^3 kT / h\nu c^2 = 2\nu^2 kT / c^2 \quad (4)$$

(for integration over frequency)

Similarly, the approximation can be applied to the wavelength form of Planck's Law:

$$B_\lambda(T) = 2kT / \lambda^2 \quad (5a)$$

for integration over frequency, or

$$B_\lambda(T) = 2ckT / \lambda^4 \quad (5b)$$

for integration over wavelength.

A very significant use of this approximation is that microwave monochromatic radiance is directly proportional to temperature in equations (4) and (5). Our dimensional analysis indicated that the higher order terms could be safely neglected. Indeed, Ulaby mentions that the Rayleigh-Jeans approximation yields values within 1% of the Planck

equation for frequencies of less than 117 GHz. Since the highest frequency observed by the sensor in this research is 87 GHz, it should be acceptable to use this approximation.

Non-Blackbody and Atmospheric Effects

Given equation (4) above, it should now be a simple matter of choosing a frequency in the microwave range, correlating the observed brightness temperature with surface temperature, calculating the coefficient $2\nu^2k/c^2$, and disseminating flawless surface temperature readings based on microwave radiation. However, equation (4) is an approximation. We must now step back and examine the flaws in our assumptions.

The first problem is, the earth is not a blackbody. That is, it does not absorb all radiation perfectly and emit the radiation perfectly in accordance with Kirchhoff's Law (Fleagle and Businger, 1980). To describe the emission properties of a non-black body, a coefficient of emissivity ϵ is normally used to relate the actual radiance of a body at a given temperature to the amount the body would radiate if it were a black body (Fleagle and Businger, 1980). This itself would not be so bad if emissivity were a single constant, but it is not. Emissivities vary as a function of wavelength and temperature (Fleagle and Businger, 1980). Worse still, emissivities can change considerably based on the molecular structure of the surface (Ulaby, 1986). While the latter can be overcome when the surface sensed is homogeneous, it can become quite troublesome for composite surfaces, such as those which are on land (McFarland, 1991).

Further complicating the matter is that a non-blackbody surface reflects radiation it does not absorb. Assuming no radiation is transmitted through the body, the emissivity plus the reflectivity equal one. In other words, if a body has an emissivity of .65, it

would have a reflectivity of .35. The result of this is to introduce another factor that we must take into account in a radiative transfer equation.

Thus, emissivities can vary considerably on land in both space and time. The composition of the earth's surface can vary considerably in a few kilometers, while precipitation can alter emissivities and resultant detected radiation considerably over a short time. Indeed, research has been done to correlate rainfall rates with reductions in detected radiation (Conner and Petty, 1998). This brings us to another factor that affects the amount of radiation reaching a sensor: the intervening atmosphere.

While we made the original assumption that all radiation emitted in the direction of the sensor would reach that sensor, clearly this is not the case. There is still the matter of absorption, emission and scattering of microwave radiation by the atmosphere. Fortunately, since the composition of the atmosphere is relatively constant up to 90km above sea level with the exception of water vapor content (Ulaby, 1981), most attenuation due to absorption can be taken into account relatively easily. The remaining variances we must take into account come from the water vapor absorption and emission in the 22.2 GHz and 183.3 GHz bands (Ulaby, 1981) and scattering due to suspended water droplets and other hydrometeors (Ulaby, 1981).

Finally, we implicitly made the assumption that the surface of the earth was smooth and that radiation would be transmitted toward the sensor isotropically. Because the earth's surface is rough, the angle at which the surface will radiate will not always be directly away from the center of the earth; parts of the surface will radiate at varying intensities relative to the vector from the earth's surface to the sensor. The result is

diffusion of the radiation, resulting in a reduction in the radiance sensed by a radiometer (Ulaby, 1981).

Now that the nature of the problem has been explained, we will now take some time to discuss the history of remote sensing which leads us to the present state of Passive Microwave Radiometry. The information in the next section is paraphrased from Section 1-2 of Ulaby (1981).

Historical Context

Microwave radiometry can be traced back as far as Heinrich Hertz's first radio experiments in 1886. In a test of Maxwell's electromagnetic theory, Hertz constructed resonators at a frequency of 200 MHz, which is quite close to the microwave portion of the spectrum. There followed in the early 20th Century many experiments in the radio portion of the spectrum, involving continuous and pulse wave radio detection and ranging (RADAR) devices. In the 1920s, the U.S. Naval Research Laboratory conducted experiments to detect ships and aircraft, while other researchers used radio pulses to measure the height of the ionosphere.

The development of radar continued in the 1930s and 1940s. The advent of World War II hastened radar development, including a long-wave system that was deployed in aircraft. By 1946, radars operating at frequencies of 3, 10 and 24 GHz were in service and producing images of the ground. It was noted that the 24 GHz band was not always effective because of the tendency of water vapor to absorb radiation of that frequency (24 GHz is close to the 22 GHz water vapor absorption feature; pressure broadening leads to significant absorption at 24 GHz as well).

By the 1950s, the side-looking airborne radar (SLAR) was developed. With this radar and its long antenna, images produced were of finer resolution. Most SLAR systems operated at frequencies of 10 GHz, 16 GHz, and 35 GHz, though some operated at even higher frequencies. One of these systems, the AN/APQ-97, was declassified in 1964. This images created from this system over the CONUS in 1965 and 1966 were still being studied decades later.

Another major improvement was the development of synthetic aperture radar, which improved image resolution even further. With the dawn of the Space Age, proposals were drawn up to place synthetic aperture radars into space. The lag from proposal to action was considerable, however, as the first such radar launched was on Seasat in June of 1978.

In contrast to radar, or active microwave (mw) remote sensing, is passive mw remote sensing. In other words, rather than emitting a pulse of radiation at its target and recording the amount of radiation reflected, a passive sensor measures the amount of radiation naturally emitted from its target. The first spaceborne passive microwave radiometer (PMR) to acquire data did not acquire data from Earth, but from Venus. In 1962, the Mariner 2 space probe orbited Venus with a two-channel microwave radiometer aboard. The first orbiting platform to acquire such data for Earth was the Cosmos 243 satellite, launched by the Soviet Union in 1968. The first American satellite with such capabilities was Nimbus 5, launched by the National Oceanographic and Atmospheric Administration (NOAA) in 1972.

The first spaceborne PMR systems launched by the US military were incorporated in its series of Defense Meteorological Satellite Program (DMSP) polar orbiting

satellites, the first of which was launched in 1978 and was used to recover atmospheric temperature profiles (Ulaby, 1981). The First Special Sensor Microwave Imager (SSM/I), the radiometer studied in this research, was aboard the DMSP satellite F8, launched in 1987 (Hesser, 1995). Until recently, most PMR research concentrated on atmospheric temperature profiles and wind speed over smooth surfaces. The first attempt to correlate PMR data with surface temperatures was by McFarland, et al. (1991) in their development of the Calibration/Validation (CV) algorithm, which sorted data by land type and then calculated a surface temperature.

Remote sensing of land surface temperature is of special interest to the military for two reasons. First, accurate surface temperatures would lead to improved input for computer forecast models. Second, the ability to know the surface temperature gives the ground commander a tactical advantage in preparation for action in a data-sparse or enemy held area. For example, knowledge of the land surface temperature can assist in determining the times at which infrared sensors will effectively detect various targets. Since this research concentrates on the use of the SSM/I to this end, the next section provides information on the DMSP program and the SSM/I.

DMSP and the SSM/I

DMSP satellites are in a near polar orbiting, sun synchronous orbit at an altitude of approximately 830 km above the earth. Each satellite provides twice-daily global coverage and has an orbital period of about 101 minutes. Visible and infrared sensors collect images of global cloud distribution across a 3,000 km swath during both daytime and nighttime conditions. The coverage of the microwave imager is one-half that of the

visible and infrared sensors, thus the polar regions above 60° latitude are imaged on a twice daily basis, but the equatorial region are viewed on a daily basis (NGDC, 1998a).

The SSM/I instrument consists of an offset parabolic reflector that is 24 x 26 inches fed by a seven-port horn antenna. The reflector and feedhorn are mounted on a rotating drum that contains the radiometers, digital data subsystem, mechanical scanning subsystem, and power subsystem. A small mirror and a hot reference absorber are mounted on the assembly for calibration purposes.

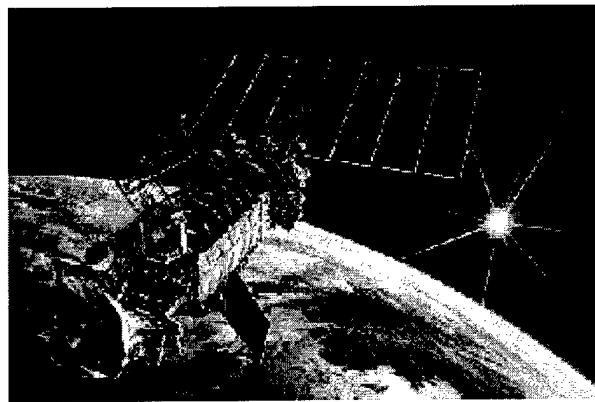


Figure 2: Schematic of a DMSP Satellite

The instrument sweeps a 45° cone around the satellite velocity vector so that the Earth incidence angle is always 54° . Data are recorded when the antenna beam intercepts the Earth's surface. The channel footprint varies with channel number (or frequency), position in the scan, along-scan or along-track direction, and altitude of the satellite. The 85 GHz footprint is the smallest at 13 x 15 km and the 19 GHz footprint is the largest at 43 x 69 km. Because the 85 GHz footprint is so small, it is sampled twice as often, i.e. 128 times a scan. One data cycle consists of 4 85 GHz scans and 2 scans of the 19, 22

and 37 GHz channels. The complete cycle takes 28 seconds and it must be complete to process the data (NGDC, 1998b).

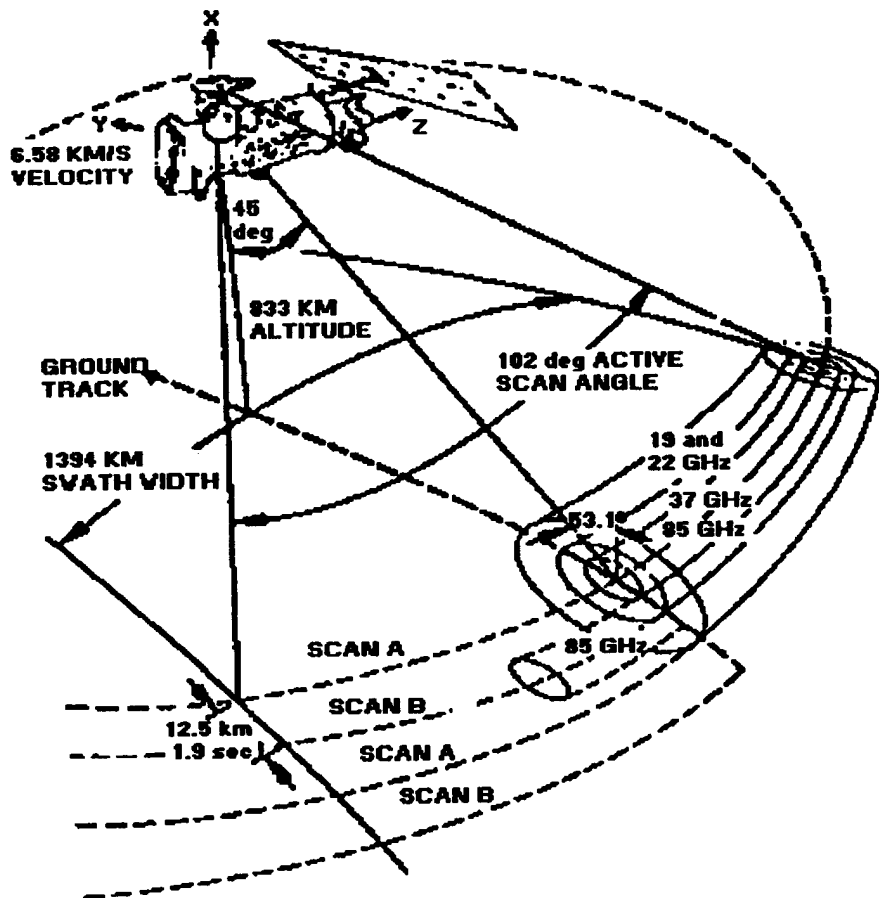


Figure 3: SSM/I Scan Geometry (Adapted from Hollinger, 1983)

As we can see in figure 4, the SSM/I scan frequencies were chosen for a reason. The 19.3, 37 and 85.5 GHz channels are in electromagnetic “window” regions, while the 22.2 GHz channel is in the middle of a water vapor absorption band and is thus highly sensitive to changes in water vapor content. In addition, the 85.5 GHz channel is highly

sensitive to scattering and can be used to detect scattering patterns associated with rainfall (Conner and Petty, 1998).

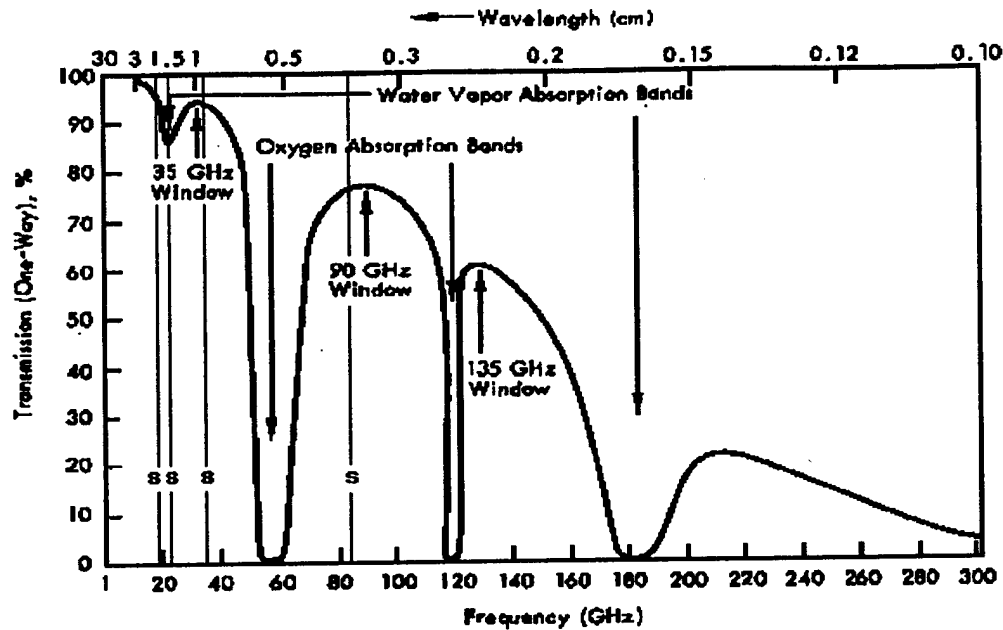


Figure 4: Percentage Transmission through Clear Atmosphere to Space (Adapted from Ulaby, 1981)

Now that we have reviewed the DMSP satellites and the SSM/I instrument, we will next look at the realistic problem of retrieving land surface temperatures from satellite-derived microwave brightness temperatures.

The Inverse Problem

If we take into account all of the factors we mentioned in our “Radiative Transfer” primer earlier, using Hollinger (1983), Rees (1990) and Ulaby (1981) as guides, we can incorporate the apparent brightness temperature into a radiative transfer equation (RTE), which relates the measured brightness temperature at a certain frequency to the desired surface temperature. The equation is rather involved (Harris, 1998):

$$T_{ap}(H) = \varepsilon T_0 e^{-\tau} + r T_{sky} e^{-2\tau} + \int_0^H \kappa_e T_{a-up} e^{-\tau} dz + \left(\int_0^H \kappa_e T_{a-down} e^{-\tau} dz \right) e^{-\tau} \quad (6)$$

where

T_{ap} = Apparent brightness temperature at satellite height H

ε = Emissivity of ground

T_0 = Physical temperature of ground

$e^{-\tau}$ = Atmospheric reduction factor

τ = Optical depth above level z

r = Reflectivity of the ground

T_{sky} = Brightness temperature of the "sky" (i.e. extraterrestrial radiation sources)

κ_e = Atmospheric extinction coefficient at level z

T_{a-down} and T_{a-up} = Physical temperature of an atmospheric layer of thickness dz at level z

In other words, the RTE shows that the apparent brightness temperature at the sensor, is a function of (a) the brightness temperature contribution by the surface, i.e. the emissivity times the blackbody brightness temperature, further reduced by atmospheric attenuation; (b) extraterrestrial background radiation, reflected by the earth and twice attenuated by the earth's atmosphere (once in and once out); (c) upward atmospheric emission, attenuated by the portion of the atmosphere between the emission point and the sensor; and (d) downward atmospheric emission, reflected by the earth and attenuated by the appropriate amount of atmosphere.

Clearly, if we knew a, b, c, and d, we could easily calculate the apparent brightness temperature. The problem lies in that we know the apparent brightness temperature and want to find the surface temperature. Such an "inverse" problem does not yield itself to straightforward analytical solution (Ulaby, 1986). Therefore, other methods such as statistical methods must be employed.

The General Linear Model

Though we could theoretically solve our problem numerically, there are too many variable parameters to do so experimentally. However, we do not need to solve the RTE. Instead, we can gather a lot of brightness temperatures and corresponding surface temperatures. This abundance of data lends itself quite well to statistical methods such as Multiple Linear Regression (Neter et al., 1983).

The general linear regression model assumes (a) there exists a linear relationship between the random variable Y (surface temperature) and a linear combination of other variables (channel brightness temperature), and (b) the value of Y minus the expected value of Y (or residual) can be represented by a normal distribution of mean 0 and some set standard deviation (Neter et al., 1983). In the case of this research, a linear brightness temperature-surface temperature relationship and Gaussian distribution of temperature deviation is reasonable (Ulaby, 1986). Further, the large number of data sets analyzed in this research means we can invoke the Central Limit Theorem, which allows us to assume a Gaussian distribution of parameters not taken into account in the regression model (Wilks, 1993), thus allowing us to satisfy assumption (b).

Given these assumptions, we can view the relationship between a single surface temperature observation and the seven corresponding channel brightness temperatures as given by the following equation:

$$Y = \beta_0 + \beta_1 X_1 + \beta_2 X_2 + \dots + \beta_7 X_7 + \varepsilon_i \quad (7)$$

An easier way to look at the above equation is in matrix format. Thus if we define vectors \mathbf{Y} , $\boldsymbol{\beta}$, and $\boldsymbol{\varepsilon}$; and a matrix \mathbf{X} as follows:

$$\mathbf{Y} = \begin{bmatrix} Y_1 \\ Y_2 \\ \dots \\ Y_n \end{bmatrix} \quad \mathbf{X} = \begin{bmatrix} 1 & X_{11} & \dots & X_{17} \\ 1 & X_{21} & \dots & X_{27} \\ \dots & \dots & \dots & \dots \\ 1 & X_{n1} & \dots & X_{n7} \end{bmatrix} \quad \boldsymbol{\beta} = \begin{bmatrix} \beta_0 \\ \beta_1 \\ \dots \\ \beta_7 \end{bmatrix} \quad \boldsymbol{\varepsilon} = \begin{bmatrix} \varepsilon_1 \\ \varepsilon_2 \\ \dots \\ \varepsilon_n \end{bmatrix}$$

we could rewrite equation (7) as (Neter et al., 1983)

$$\mathbf{Y} = \mathbf{X} \boldsymbol{\beta} + \boldsymbol{\varepsilon} \quad (8)$$

where

\mathbf{Y} is a vector of surface temperature observations

$\boldsymbol{\beta}$ is a vector of coefficients

\mathbf{X} is a matrix of brightness temperature values

$\boldsymbol{\varepsilon}$ is a vector of independent normal random variables with expected value of 0 and variance $\sigma^2 \mathbf{I}$ (where \mathbf{I} is the Identity Matrix)

Knowing $\boldsymbol{\beta}$, we can retrieve \mathbf{Y} (the vector of surface temperatures) from \mathbf{X} (the vector of brightness temperatures). Unfortunately, we cannot use equation (7) to calculate the “true” coefficients because we do not know what the error values are. Fortunately, we can use the method of least squares (Devore, 1995) to estimate the regression coefficients $\boldsymbol{\beta}$. In matrix form, Neter describes the calculation of the vector of estimated coefficients \mathbf{b} (an estimate of $\boldsymbol{\beta}$) as:

$$\mathbf{b} = (\mathbf{X}^T \mathbf{X})^{-1} \mathbf{X}^T \mathbf{Y} \quad (9)$$

In our experiment, we are dealing with thousands of data sets and seven brightness temperature channels to regress. Inverting and transposing such matrices by hand would be highly cumbersome. Fortunately, there exist many software packages to make these calculations for us. The software package I used was S-Plus 4.5 by Mathsoft, Inc. (1997).

Stepwise Linear Regression

Whenever possible, it is desirable to remove variables from a regression in order to simplify the math involved. When the contribution of a certain variable X only gives a marginal contribution to the multiple R-squared value (for further explanation, see section 13.4 of Devore, 1995) of the regression estimate, that variable can be removed without significantly reducing the accuracy of the regression. One of the most common methods of removing variables in this manner is stepwise linear regression. The method of stepwise regression develops a series of regression models, at each step adding or deleting a variable (Neter et al., 1983). Fortunately, the S-Plus software has the capability to perform stepwise regression.

It is important to note, however, that stepwise linear regression has its limitations. Among the most significant to our research is that stepwise regression will occasionally arrive at an unreasonable subset of variables when the overall variable set is highly correlated (Neter et al., 1983). Since the full set of brightness temperatures can have correlation as high as .9 at times (McFarland, 1991), it will be important to keep an eye on the “aptness” of the model. Among the methods used to test regression aptness is to check that the residuals do not deviate significantly from normality (Neter and

Wasserman, 1974). This can be done with a number of plots, which are available in S-Plus. Such plots of the regressions performed in this research will be shown in Chapter IV and Appendix B.

Antenna Temperature vs. Brightness Temperature

The SSM/I sensors do not detect brightness temperature directly. Rather, the sensors measure what is known as antenna temperature. In order to explain this, we must delve briefly into antenna theory.

The best way to think of a passive antenna is as a wire. It functions to guide electromagnetic waves along itself (Ulaby, 1981). The radiometer works in that it measures the voltage change in various frequencies along the antenna. Given a bandwidth and the physical characteristics of the antenna, the voltage counts transmitted by the satellite can be translated into brightness temperatures. For the SSM/I instrument, Air Force Weather Agency (AFWA), Offutt AFB, translates the raw counts into brightness temperatures and places them into a Sensor Data Record (SDR). It is important to keep in mind that the brightness temperatures studied did not come directly from the satellite but were first converted from voltage counts; this introduces another possible source of error into the research, calibration error.

The Calibration/Validation (CV) Algorithm

The algorithm studied in this research is the CV algorithm. For a given "scene," this routine first looks at relationships between the seven channel brightness temperatures in order to determine a land type. The brightness temperature ranges relevant to the

respective land types were determined experimentally by observing channel brightness temperature relationships over known land types (Hollinger, 1983). The CV program first separates data into 8 different land types: dry, arable soil; moist soil; semidesert; desert; dense vegetation; mixed water and vegetation; light vegetation, and wet soil. Following is an example of a land type-sorting algorithm for the “dry, arable soil” land type:

If $(V22 - V19) \leq 4.0$ *and*
 $4.0 < (V19 + V37) / 2 \leq 9.8$ *and*
 $(V37 - V19) \geq -6.5$ *and*
 $-5.0 \leq (V85 - V37) < 0.5$ *and*
 $(H85 - H37) < 4.2$ *then*

land type = dry arable soil

Where variables are by polarization and frequency, e.g. “V22” is the brightness temperature measured for vertical polarization at 22 GHz

In the original CV algorithm, these land types were then recombined into four more general land types: dense vegetation, agricultural / range, moist soils, and dry soils. Multiple linear regression was performed and coefficients were calculated for each land type (McFarland, 1991). In this research, we will concentrate on the eight original land types, plus the data points for which the CV algorithm could not determine a land type.

Indicator Variables and Qualitative Regression

This research investigates two different sets of data: one set consisting of data from the F10 and F13 DMSP satellites, and another set from the F14 DMSP satellite. Part of the research involves determining if there is a statistically significant difference

between the regression coefficients obtained for the two data sets. The simplest method to perform such a qualitative regression is the use of an indicator variable (Neter et al., 1983).

An indicator variable is a variable that identifies a category of data. In this case, our categories are F10/F13 data and F14 data. For our research, we may create a variable with the values 0 and 1: 0 for the F10/F13 data and 1 for the F14 data. Regression can then be performed on the combined (F10/F13/F14) data set, including the indicator variable with the other relevant variables in the regression. The Null hypothesis will be that the coefficient of the indicator variable in the regression will be zero, i.e. the regression functions of the two data sets are identical. The Alternative hypothesis will be that the coefficient of the indicator variable will not be zero. A standard t-test or partial-F test can be performed to determine whether or not to reject the Null hypothesis. For further information on the use of indicator variables, see Chapter 10 of Neter et al. (1983).

Earlier in this chapter, most of the sources of error were introduced. However, it is always beneficial to have listed potential sources of error in the same place. In the next section, these sources will be summarized.

Sources of Error

Given the sizes of the SSM/I channel “footprints,” the most glaring source of error is the potential mixture of land types in a single SSM/I measurement. The land type determination of the CV algorithm is far from exact, but even if it were exact, brightness temperatures are taken over areas greater than 100 square kilometers. A number of

varying land types viewed within a given pixel will lead to several surface emissivities contributing to a single measurement.

Another source of error is that we are using surface temperature observations to correlate with satellite-measured brightness temperatures. These two measurement methods do not always give consistent results. For example, the ground-measured air temperature trends since 1979 differ significantly from those observed by satellite-borne PMR (Hurrell and Trenberth, 1996). This difference of instrumentation may introduce a systematic error to our results.

Another source of error is the assumption of a linear relationship between brightness temperature and surface temperature. While the Rayleigh-Jeans approximation lends validity to the assumption of a linear relationship between terrestrial microwave radiation and land surface temperature, it only applies to one part of the RTE. There are contributions from three other parts of the RTE – two components due to atmospheric microwave radiation (one upward radiation to the sensor, and one downward radiation reflected by the earth), and one component due to reflected extraterrestrial microwave radiation. These contributions are not necessarily linear, which adds a nonlinear aspect to the problem.

A fourth source of error is the regression itself. Even if the brightness temperature-surface temperature relationship were exactly linear, because of measurement error, the regression can only calculate an approximation of the actual, ideal coefficients (Neter et al., 1983). However, the larger the regressed data set is, the more accurate the approximation to the true coefficients will be.

A fifth potential source of error is calibration error. If the calibration was not performed correctly, the conversion from radiation counts to brightness temperatures could introduce a systematic error to the calculations. It has been noted that different calibration averaging techniques and other processing can result in different antenna temperatures being calculated from the same radiation counts (Ritchie et al., 1998). The accuracy of the algorithm used to translate SSM/I radiation counts to brightness temperatures is beyond the scope of this research and will not be examined.

Still another source of error is the accuracy of the land type algorithm itself. While diagnosis of the land type sorting will not be performed in this research, it is important to note that an erroneous land type diagnosis will introduce error. Such miscategorization could be caused by a number of factors, not the least of which the presence of hydrometeors.

The effects of precipitation on microwave emissions are twofold: first, a higher liquid water amount translates to a higher brightness temperature, especially in the 19 GHz range. Second, scattering by large ice particles at high frequencies (e.g. in the 85 GHz range) reduces the amount of radiation reaching the satellite (Liu and Curry, 1998).

The final source of error is the error universal to any experiment – noise. From noise in the radiometer measurements, to noise in the measurements of surface temperature, instrumentation error will add some variability to in the results. If this noise is of a random nature, it will conform to a Gaussian distribution and be averaged out of the results through linear regression.

Related Research

An initial search for research on PMR-derived land surface temperatures only yielded the previous work done at AFIT (Harris, 1998; and Comoglio, 1997). While no additional research concerning SSM/I-derived land surface temperatures was found, there were several articles that provided background on PMR, possible sources of error, and other uses for PMR. One richly researched example was use of PMR to determine rainfall rates.

Hurrell and Trenberth (1996) examined the differences in observed trends between near-global monthly mean surface temperature anomalies and those of global Microwave Sounding Unit 2R (MSU 2R) temperatures for 1979-1995. The variability of surface-observed temperatures was found to be small over the oceans but large over the land, while MSU 2R measured variations that were much more zonally symmetric. Also, the two measurement systems gave greatly dissimilar responses to volcanic eruptions, the El Niño Southern Oscillation (ENSO), and changes in stratospheric ozone. Hurrell and Trenberth conclude that most of the differences can be attributed to physical differences between the two measurement techniques. They emphasize that neither technique is more correct, rather that both techniques give a different perspective on the same events.

Ritchie et al. (1998) investigated differences in PMR-derived rainfall-rate products from NGDC and Fleet Numerical Meteorology and Oceanography Center (FNMOC), which used identical SSM/I data. The differences were traced to different calibration averaging techniques and other processing methods, which yielded different antenna temperatures from the same data sets. The effects of these temperature differences were then examined by generating rain rates using the Goddard Scattering

Algorithm. The conclusion was that it was possible to infer greater rain rates from a cold bias introduced in antenna temperature processing. Conversely, rain rates would be lower if the antenna temperature processing yielded a warm bias.

Liu and Curry (1998) examined the effects of hydrometeors on microwave emissions. In their research, they attempted to determine if a relationship existed between polarization differences (D) at 19 GHz and polarization corrected temperature (PCT) at 85 GHz. 5° latitude X 5° longitude regional means of these parameters over global oceans were calculated for areas of no precipitation, light precipitation, and heavy precipitation. In the case of no precipitation, a small variation of PCT could be achieved by changing the weights given to the polarization brightness temperatures in the 85 GHz channel. For light precipitation, the relationship between D and PCT was latitude dependent. No clear latitudinal dependence was found for heavy precipitation. Liu and Curry conclude that the value of the D-PCT slope can be used to help categorize precipitation types, which may be useful in determining a specific algorithm best used for precipitation type.

Conner and Petty (1998) compared SSM/I rain rate retrieval methods over the Continental United States. The researchers compared three experimental rain-rate algorithms (sorted by land type) with two existing SSM/I rain rate algorithms, using hourly rain gauge reports and 10-cm radar data for ground truth. Results of the research were inconclusive: the five algorithms yielded similar results, with no algorithm showing itself to be superior.

Kidd et al. (1998) reviewed the performance of rainfall rate retrieval algorithms established by statistical relationships and empirical calibration. The advantages of

statistical-empirical algorithms were found to outweigh the disadvantages, though developers are aware of the limitations of such algorithms. Physically-based algorithms, they conclude, are not likely to improve until the intricacies of the physical relationships are better understood.

Ferraro et al. (1998) set forth a methodology to screen land-related effects from SSM/I precipitation retrieval algorithms. They found the complicated interaction of earth-emitted microwave radiation with various land types and atmospheric variations made the development of a single global screening methodology very difficult. For this reason, they recommend development of screening methodologies on a regional basis.

Wentz and Spencer (1998) developed a physically-based algorithm for retrieving rain rates from SSM/I measurements over oceans. The algorithm uses a beamfilling correction based upon liquid water absorption coefficients at 37 GHz and 19 GHz to correct the underestimation of rainfall rates by other physically-based techniques. The algorithm simultaneously calculates wind speed, columnar water vapor and liquid water content, rain rate, and effective radiating temperatures for upwelling radiation. The root mean square difference between retrieved water vapor value and radiosonde-measured value was 5 mm. The algorithm was still found to underestimate rainfall rates in the tropics.

Documentation on the SSM/I sensor by Hollinger (1983) contained a summary description of the SSM/I instrument, as well as descriptions of the geophysical models, the interaction model, the retrieval technique, and the climatology used for the SSM/I environmental retrieval algorithm. McFarland (1991), who investigated the brightness temperature behavior and polarization differences among various land types, conducted

the research that led to the CV algorithm. McFarland used SSM/I brightness temperatures obtained for specific locations on earth of a known land type. From these data, he derived a set of logical if-and-then statements (including the sample statements shown earlier in this chapter) for determination of 14 distinct land types (9 of which are still used by AFWA in the CV algorithm) from the 7 channel brightness temperature measurements. McFarland next used multiple linear regression to calculate algorithms to correlate SSM/I measurements and land surface temperatures for each of four general land type categories. For this portion of the research, which spanned four days in August 1987, SSM/I readings from the F8 satellite over the US Western Desert and Central plains were matched with high/low temperature observations from the federal climatological network.

Other research found of relevance to this thesis was a paper investigating land surface temperature determination from satellites (Prata, 1994), in which the Advanced Very High Resolution Radiometer (AVHRR) and the Along Track Scanning Radiometer (ATSR) were used to compare IR emissions with surface temperatures over Continental Australia. The work concluded that an algorithm that took into account climatological temperature and water vapor profiles could yield accurate temperature measurements.

Schmugge and Schmidt (1998) also used an AVHRR sensor aboard the NOAA-9 satellite to measure the surface temperature during the First ISLSCP (International Satellite Land Surface Climatology Project) Field Experiment (FIFE), conducted over grassland terrain in central Kansas in 1987. The AVHRR-derived values were corrected for atmospheric effects and compared to broadband temperature readings at 10 sites and to the thermal channel of an NS001 sensor aboard a C-130 aircraft. The AVHRR values

were found to be 5° to 6°C warmer than the average of the ground measurements. The researchers attributed the difference to the location of ground measurements being skewed toward well-vegetated surfaces.

Betts and Ball (1998) performed a study confirming earlier research regarding the diurnal and seasonal variation of surface albedo. One of the findings was that soil heat flux is reduced at night when soil is drier.

Summary

Measurement of microwave emissions to determine land surface temperature is feasible but fraught with complications. Use of the Rayleigh-Jeans approximation can simplify the problem, but one must remain mindful of the extent to which the earth does not conform to required assumptions. The radiative transfer equation relates surface temperature to various brightness temperatures, but the equation cannot be solved easily due to its inverse nature. Given the large amount of data present, statistical methods such as multiple linear regression can be used to estimate coefficients for a solution.

The CV algorithm sorts data by land type, which can make regression more accurate. To compare data from two different satellites, an indicator variable can be generated and regressed to determine if the regression functions are identical. Sources of error are many, but with luck can be quantified via regression. Finally, very little recent research has been done on using SSM/I to calculate land surface temperatures, other than that performed at AFIT by Harris and Comoglio.

III. Methodology

Chapter Overview

This chapter explains the processing of the data into meaningful results. Satellite brightness temperature channels were consolidated into sets by time and location and then compared to surface temperature observations taken nearby at comparable times. These matched sets were then exported into files, consolidated by season, and sorted by CV to determine land types. Finally, data was exported to a PC and processed using statistical software.

The following sections will first touch upon the work done by others at AFIT (Harris, 1998; and Comoglio, 1997) and explain how the data they acquired was modified to fit the purposes of this research. There will follow a detailed discussion of the matching and sorting process performed. At the end of the chapter, there will be a discussion of the regression techniques, both quantitative and qualitative, used to determine the results of the research.

Past Work at AFIT

While the research performed in this thesis is not directly related to the work of Harris (1998) and Comoglio (1997), both the data they gathered and the FORTRAN code they wrote were quite useful in its successful completion. Comoglio started with preliminary research comparing the effectiveness of the CV algorithm with the TMPSMI (TS) algorithm. Due to problems decoding the data, he was unable to make a complete comparison of the two algorithms. Taking up where Comoglio left off, Harris gathered

additional data and completed the study, in which he concluded the CV algorithm was more accurate. Among the data gathered by Harris and Comoglio were sets of SSM/I readings decoded into brightness temperatures by AFWA (known as Sensor Data Records or SDR) and surface observations (acquired from the Air Force Combat Climatology Center [AFCCC]) for Bosnia, the continental United States, Saudi Arabia, and the Korean Peninsula. SDR readings from the F13 DMSP satellite were recorded over the four areas during August 1996, October 1996, and January-February 1997. Harris also acquired SDR from both the F13 and F14 satellites for the period of late August -September 1997, but he did not have the time to decode this data for his study. The data used in this study is summarized in Table 1 below.

Harris and Comoglio also wrote a number of useful programs and algorithms to analyze the data. While I was only able to use one of their programs directly, I was able to adapt a number of their algorithms to accomplish important tasks in my efforts. Thus, it can be said that my work was very much a team effort in concert with the efforts of Harris and Comoglio.

Table 1: Data Matches Used in Research

Satellite(s)	Date	# of Matches
F10/F13	16-Oct-96	90
F10/F13	17-Oct-96	68
F10/F13	18-Oct-96	229
F10/F13	21-Oct-96	223
F10/F13	22-Oct-96	88
F10/F13	25-Oct-96	137
F10/F13	29-Oct-96	233
F10/F13	31-Oct-96	230
F10/F13	04-Nov-99	270
F10/F13	05-Nov-96	208
F14	22-Aug-97	136
F14	27-Aug-97	211
F14	28-Aug-97	227
F14	02-Sep-97	195
F14	04-Sep-97	243
F14	16-Sep-97	239
F14	17-Sep-97	192
F14	18-Sep-97	74
F14	19-Sep-97	134
F14	22-Sep-97	107
F14	23-Sep-97	137
F14	25-Sep-97	165
F14	26-Sep-97	203
F14	30-Sep-97	318

Data Description

The SSM/I SDR data was recorded on 8mm tapes by AFWA. The files were organized such that every day of observation was in a separate directory. Inside each directory were nine binary files: one for each of the seven channels, one for the date time group of the satellite pass, and one for the identity of the satellite (See Table 2). Each file contained readings for each 64 x 64 grid cell within each of the 64 polar stereographic grid boxes (or 4096 grid cells) which cover the entire Northern Hemisphere (See Figure 5).

Table 2: Satellite Data File Names

File Type	File Name
Grid Date Time Stamp	RNXMI1_00MITT
19 GHz, Vertical Polarization	RNXMI1_00MIH1
19 GHz, Horizontal Polarization	RNXMI1_00MIV1
22 GHz, Vertical Polarization	RNXMI1_00MIV2
37 GHz, Horizontal Polarization	RNXMI1_00MIH3
37 GHz, Vertical Polarization	RNXMI1_00MIV3
85 GHz, Horizontal Polarization	RNXMI1_00MIH8
85 GHz, Vertical Polarization	RNXMI1_00MIV8
Satellite Identifier	RNXMI1_00MIID

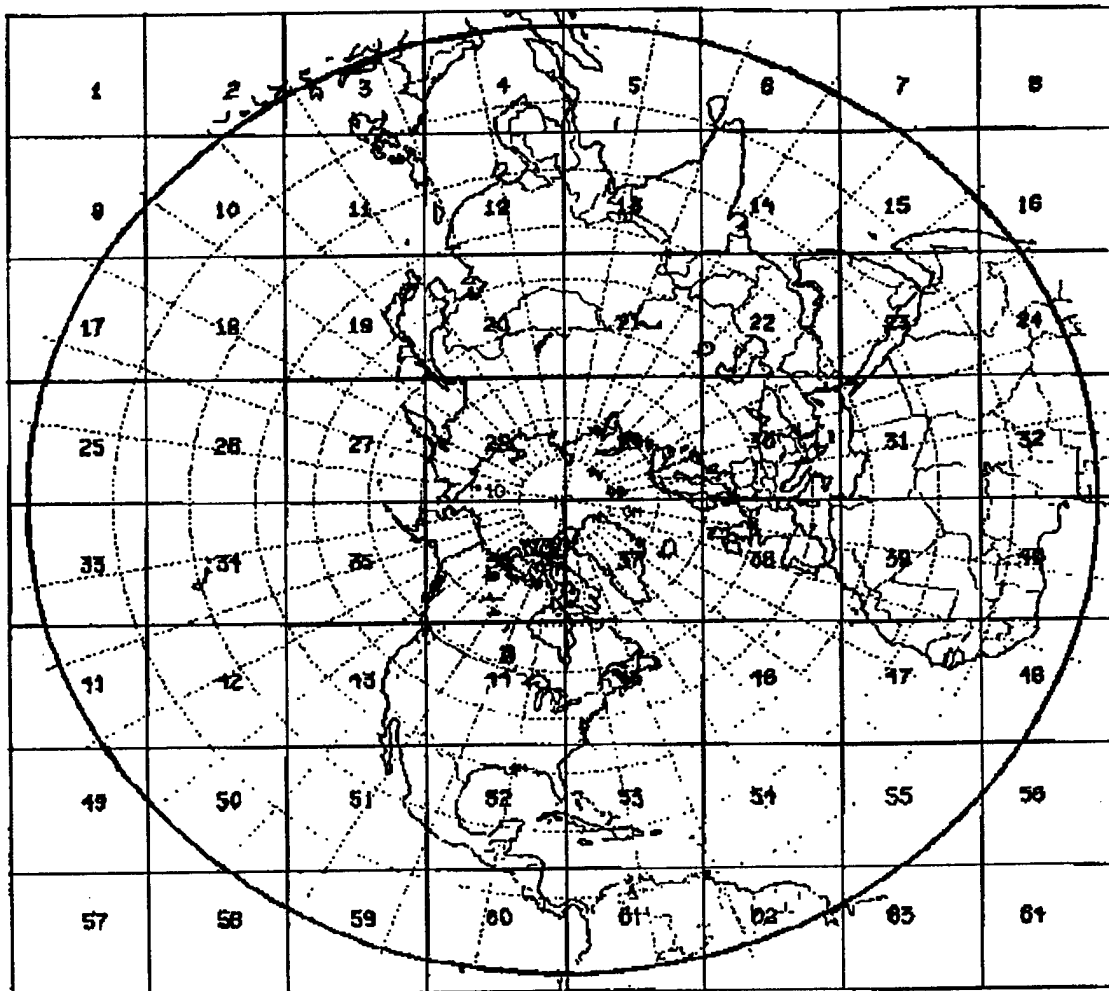


Figure 5: Polar Stereographic Northern Hemisphere Grid

The surface temperature data from AFCCC was sent in compressed format on 3 ½ inch disks. Each line consisted of a series of numbers, representing the World Meteorological Organization's (WMO) station number; the year, month, and day of the observation; the hour and minute of the observation in Universal time; the surface temperature in Kelvin; and the longitude and latitude of the station (See Table 3).

Table 3: Example of Data Format

STATION	YEAR	MO	DAY	HR	LAT	LON	TEMPK
470050	1996	10	01	0300	41.817	128.317	289.66
470050	1996	10	01	0600	41.817	128.317	291.66
470050	1996	10	01	0900	41.817	128.317	286.36
470050	1996	10	01	1200	41.817	128.317	280.46
470050	1996	10	01	1500	41.817	128.317	279.36

Decoding, Combining, Matching, and Sorting the Data

The four phases of transforming disparate data files into a group of usable matched data sets are: decoding, combining, matching, and sorting (See Figure 6 for a flow chart which outlines the four step process). For F10/F13 data already analyzed by Harris (1998), the first phase was already accomplished; the August 1996, October 1996, and January/February 1997 SSM/I SDR files were already decoded into ASCII files from binary files. The following few paragraphs outline the data analyzing process, first for the three seasons outlined above, and then for the late August/September 1997 data not previously analyzed.

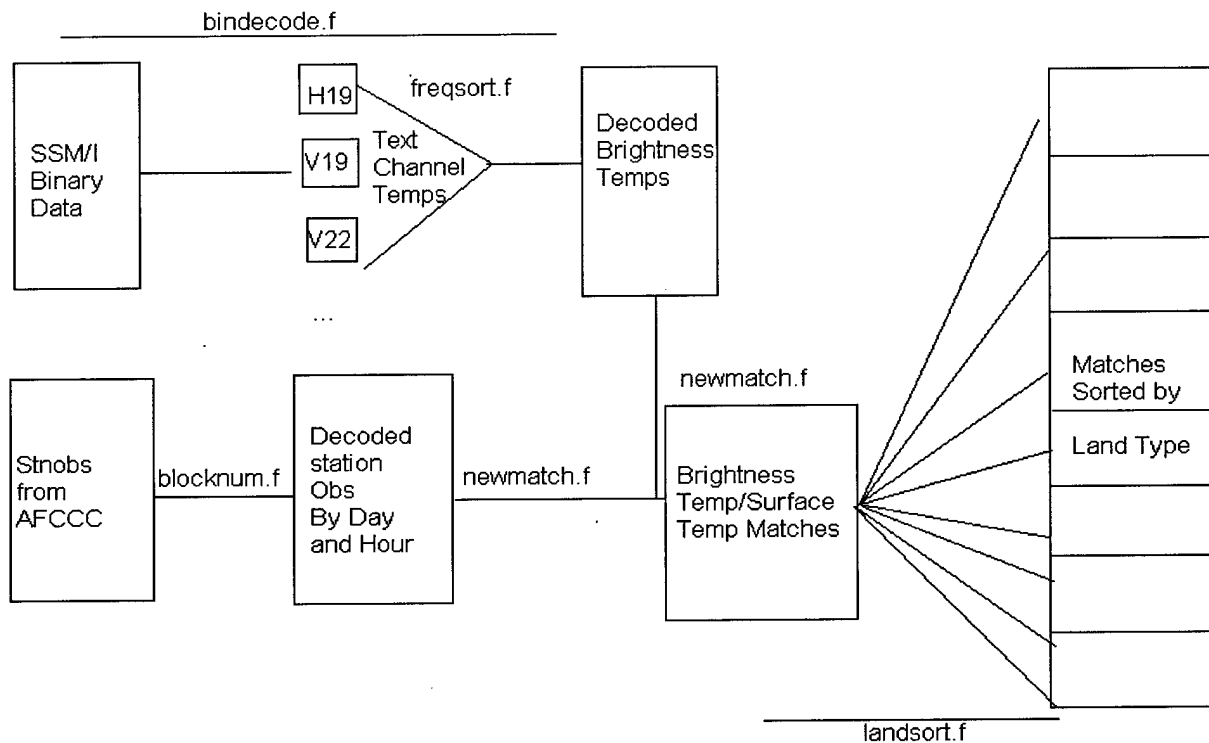


Figure 6: Methodology Flow Chart

In the data already analyzed by Harris (1998), some of the groundwork had already been done. However, Harris compared data *pairs* of CV or TS algorithm temperature with surface temperature, whereas this research matched data *sets* of the seven channel brightness temperatures with corresponding surface temperatures. Further, while Harris implicitly sorted by land type when he used the CV and TS source code to calculate the algorithm temperatures, he had no need to sort the output by land type to accomplish his goals. Thus, while this research used the same raw data, it needed to be manipulated in a substantially different manner than previous research had done

Nevertheless, the F10/F13 SSM/I SDR data having already been decoded gave the research a considerable boost. For the August 1996, October 1996, and January/February 1997 data, the binary data had already been decoded into ASCII. Thus, for this data,

phase one was already complete. For phase two, a short FORTRAN program was written to combine the seven separate channel temperature files for each day into one file per day. The record format of the new daily file was: seven channel brightness temperatures, followed by the three grid coordinates, referred to hereafter as “i”, “j”, and “k” coordinates.

The third phase was to match the sets of channel temperatures to a surface observation nearby in both space and time. For determination of spatial proximity, the earlier criterion of Harris (1998) and Comoglio (1997) were used: the surface station and SSM/I measurement coordinates must be no more than 1 grid point apart (see figure 7). For ease of calculation, so-called “superneph” coordinates were used – that is, the “i,” “j” and “k” coordinates converted into 512 x 512 “SI” and SJ” coordinates. For the surface temperature observations, a FORTRAN program written by Harris and Comoglio was used to translate the latitudes and longitudes into “superneph” coordinates. After the surface observations were properly formatted, a new FORTRAN program performed the matching with corresponding brightness temperatures by space and time. While much of the code was original, many algorithms were adapted from a previously existing program (Harris, 1998). The matching program first looked at the Julian day and time of the observation at each grid point. If the Julian day matched the day being examined (i.e. the program automatically threw out any data from passes on previous days), it then opened the observation file for the appropriate hour’s observations. The program then converted the brightness temperature i, j, and k coordinates to SI and SJ grid coordinates, and compared them to the SI and SJ coordinates of each observation. If the coordinate sets

were within one grid point of one another, the program saved the matched data set to a match file. This process continued until all grid points had been examined in this way.

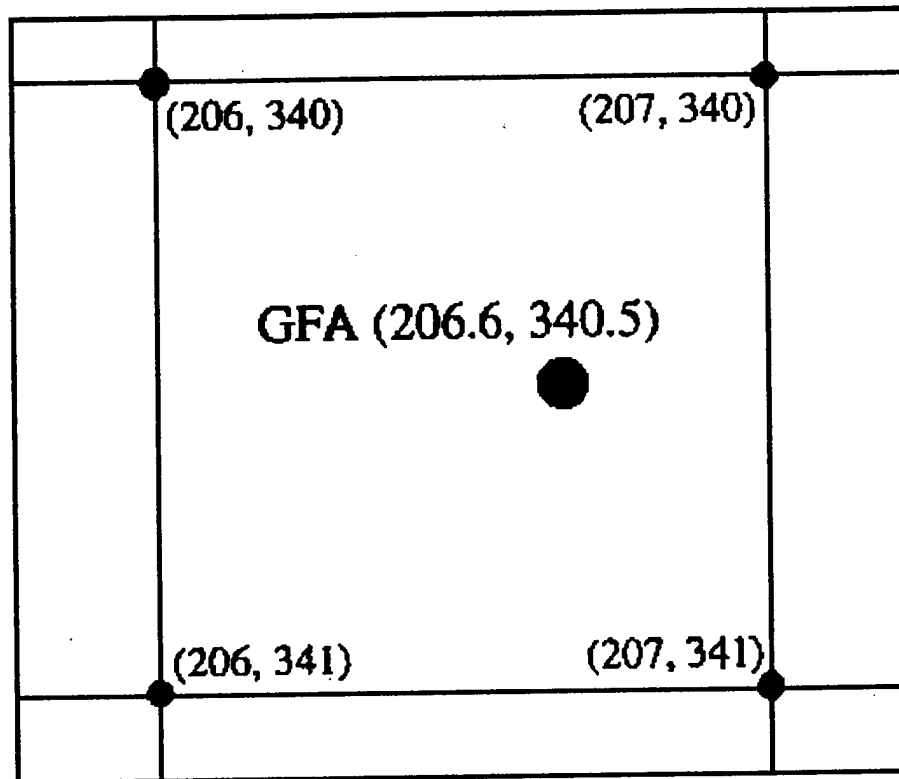


Figure 7: “Superneph” grid over Malmstrom AFB, MT, ICAO “GFA”
(From Harris, 1998)

Once all data had been matched, phase four sorted the matched data by CV land type. This was done by a FORTRAN program. While much of the code was original, the CV land sorting algorithms were taken from the existing calval FORTRAN program (see Harris, 1998). This program created nine files: one for each of the eight CV land types, and a ninth for those observations not fitting any of the land types. The specific land type algorithms are listed in Appendix C. After the program was run for each day, a UNIX text editor was used to combine the daily data into “seasonal” files: Summer 1996, Fall

1996, and Winter 1997. (Note: Harris's original data was further sorted by "CONUS" and "overseas" region. While some analysis was done on the regions separately, this researcher eventually decided not to sort the data by region.) After the data was manipulated as described above, the data sets were transferred to a PC, where the files were imported into the statistical program "S Plus" for analysis.

After the original data was analyzed, the research turned to the Fall 1997 data not analyzed before. Unlike the data described earlier, this data was still in binary form. Therefore, the transformation process had to start with phase one.

Having learned some lessons from the original run through, the process for analyzing the F14 data was streamlined. First, phases one and two were accomplished with a single FORTRAN program. This program opened all appropriate files for a given day, then wrote the i, j, and k coordinates; day and time of observation; the satellite ID number, and the seven channel temperatures for each grid point. For the purposes of saving storage space, only the grid boxes over CONUS, Saudi Arabia, Bosnia, and Korea were decoded and saved in ASCII format.

There were only slight differences in the process for phases three and four for the F14 data. Synoptic temperature observations were again decoded using an existing FORTRAN program written by Comoglio (1997) and Harris (1998), which this researcher modified slightly.

The matching process was again performed by a FORTRAN program, which was only slightly modified for the F14 data. Specifically, the match program was rewritten to identify the satellite ID of each reading. If the satellite ID number did not equal 48, the ID number assigned to the F14 satellite (Coxwell, private communication, 1998), the

matched data set was not saved to the appropriate file. This was done to ensure the new data would indeed consist entirely of brightness temperature data from the F14 satellite. In another lesson learned from the first analysis, the daily files were merged into a single data file before the data was sorted into many different land type files.

As was done with the earlier data sets, a FORTRAN program was used to sort the matched data sets into land type categories. An additional parameter was added to the end of each data set: an integer "1" to identify the new data as F14 data. As was done with the earlier data, the files were then transferred to a PC for analysis. Separate files were created, combining the F10/F13 data from Fall 1996 and the F14 data for each land type, and adding a "0" to the F10/F13 data in a new column to match the "1" for the F14 data. The data was then ready for both quantitative and qualitative regression.

Statistics Used

This research will use the statistical methods of multiple linear regression (MLR) and stepwise linear regression. These methods are outlined in the "General Linear Model" and "Stepwise Linear Regression" sections of Chapter II. The assumed "true" regression equation will be in the form of equation (7), specifically as follows:

$$T_i = \beta_0 + \beta_1 H19_i + \beta_2 V19_i + \dots + \beta_7 V85_i (+ \beta_{indicator} Indicator_i) + \varepsilon_i \quad (9)$$

Where T_i is the synoptic temperature observation

$H19_i$, $V19_i$, etc represent the brightness temperature values

$\beta_{indicator}$ and $Indicator_i$ represent the qualitative regression coefficient and the indicator variable respectively.

ε_i is the residual assumed to be taken from a normal distribution of mean 0 and variance s^2 .

In equation (9) above, the parenthetical term is included in the qualitative regression to determine if there is a statistically significant difference between the F10/F13 data and the F14 data.

To analyze the quality of results of the data regression, five statistics were used: the root mean square error (RMSE, also known as the residual standard error), the root mean square predictor error (RMSPR), the multiple R squared statistic, the F statistic, and the t statistic. The RMSE was used to evaluate the variance of the fitted temperature values with respect to the synoptic temperature measurements. The RMSPR was used to cross-validate regression on another data set. The multiple R squared was used to evaluate the amount of variance explained by the multiple regression, i.e. the “goodness of fit” of the regression. The F statistic was used to test the validity of the Null Hypothesis that all regression coefficients were equal to zero. Finally, the t statistic was used to decide upon the validity of the Null Hypothesis that the true regression equations of the F10/F13 data set and the F14 data set were identical. The latter determination is important because the primary goal of this research is to determine if CV brightness temperature coefficients need to be calculated separately for each new DMSP satellite launched.

A common accuracy measure in the environmental sciences is the MSE, or mean squared error, which averages the individual squared differences between a forecasted value and an observed value (Wilks, 1995). In the case of this research, we can think of the fitted temperature value of the regression as the “forecast.” Thus, if we consider y the fitted value and o the value of the synoptic observation, the MSE for M such data pairs is

$$MSE = (1/M) \sum_{m=1}^M (y_m - o_m)^2 \quad (10)$$

The statistic RMSE, the statistic used in this research is simply the square root of MSE (Wilks, 1995).

The mean squared predictor error is a means of measuring the actual predictive capability of the selected regression model by testing its effectiveness on another data set (Neter et al., 1989). The MSPR for n^* data sets in the new (or validation) data set is

$$MSPR = (1/n^*) \sum_{i=1}^{n^*} (y_i - o_i)^2$$

If the MSPR is fairly close to the MSE based on the regression fit to the original (or training) data set, then the error mean square MSE for the selected regression model is not seriously biased and gives an approximate indication of the predictive ability of the model. If the MSPR is much larger than the MSE, one should rely on MSPR to determine how well the selected regression model will predict in the future. (Neter et al., 1989)

The R squared statistic, also called the coefficient of multiple determination, is a number between 0 and 1 which describes the proportion of total variation “explained” by the multiple regression model (Devore, 1995), or the “goodness of fit” of the regression. In other words, it is the degree to which the variance of the data is explained by the regression equation. If every data point fell exactly on the regression line, the R-squared

value would be 1. If, on the other hand, the sum of the squares of the distances from the regression line were not significantly smaller than the sum of the squares of the distances from the overall mean, the R-squared value would be very low. Typically, if an R-squared is small, an analyst will usually want to search for an alternative model that can more effectively explain data variation (Devore, 1995). While there is no agreed-upon “cutoff” value for R-squared, I consider an R-squared = .6 as the minimum value to consider the regression a “good fit.”

R-squared is calculated numerically as

$$R^2 = 1 - SSE / SST \quad (11)$$

where

$$SSE = \sum (y_m - o_m)^2 \quad (12)$$

and

$$SST = \sum (y_m - \bar{y})^2 \quad (13)$$

In equation (13), the overall data mean value \bar{y} is subtracted from each predicted value (y_m), whereas in equation (12) involves subtracting each different predicted value (y_m) from the corresponding observed value (o_m)(Devore, 1995). In other words, SSE is the sum of squared deviations about the regression line, while SST is the sum of squared

deviations about the mean value of the entire data set. MLR will minimize SSE, thereby maximizing R-squared.

The F statistic is used in a model utility test which determines if there is a useful relationship between y and the regressed predictors (Devore, 1995). For this research, F will be used to validate or reject the Null Hypothesis

$$H_0 : \beta_0 = \beta_1 = \beta_2 = \dots = \beta_7 = 0 \quad (14)$$

in favor of the Alternative Hypothesis

$$H_a: \text{Not all true regression coefficients} = 0 \quad (15)$$

F* is calculated for a multiple regression with n data points and k predictors as

$$F^* = (R^2 / k) / \{(1 - R^2) / [n - k + 1]\} \quad (16)$$

with the rejection level for the Null hypothesis (in the case of this research, a .01 probability of Type I Error, or the probability of rejecting the Null when the Null is true) being

$$F^* \geq F_{.01, k, n-(k+1)} \equiv F_{crit} \quad (17)$$

The critical value $F_{.01, k, n-(k+1)}$ can be determined either with a mathematical program such as MATHCAD, or through use of a statistical table. Figure 8 shows the critical value of

F for 7 and 92 degrees of freedom, corresponding to MLR on 100 data points and seven predictor variables.

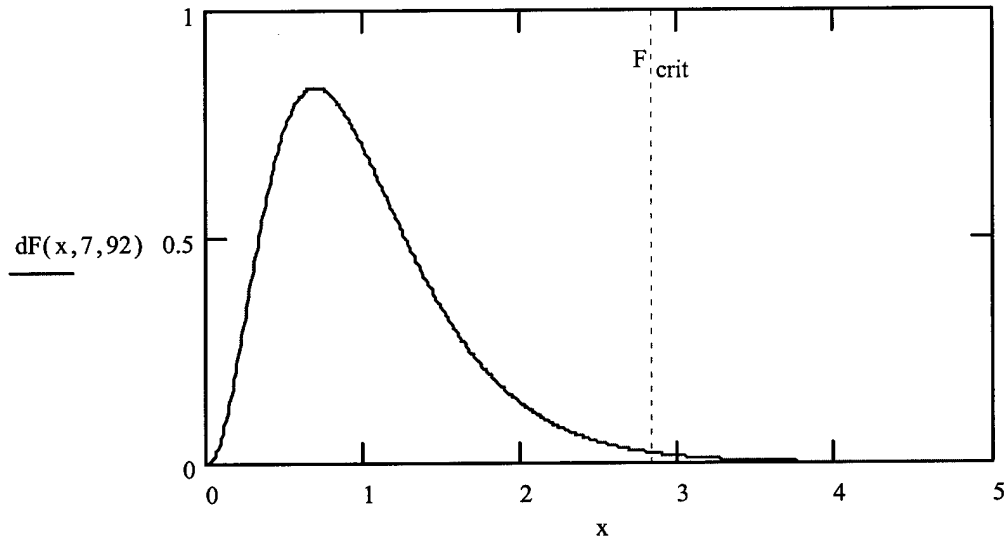


Figure 8: F distribution with 7 and 92 degrees of freedom.
Critical value F_{crit} is shown.

Since the numbers k and n will vary among the various data sets, I will not explicitly calculate the critical F value for each data set. Rather, I will measure the probability of the Null being rejected but actually being true. This value, or “P-value”, is the area under the curve of the Null’s F distribution greater than the statistic F^* . This can be expressed numerically as

$$P = \int_{F^*}^{\infty} F_{null} dx \quad (18)$$

and can be expressed graphically as shown in Figure 9.

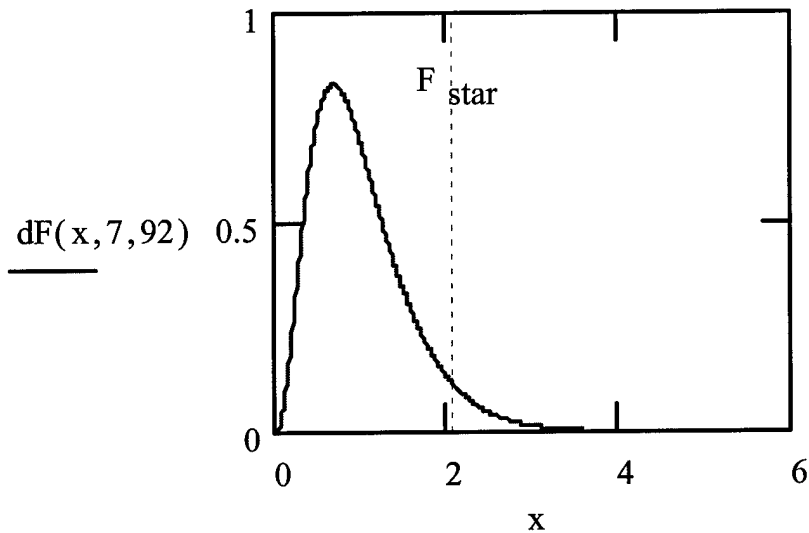


Figure 9: F distribution with 7 and 92 degrees of freedom.
P-value is the area under the curve to the right of F*.

A P-value smaller than the desired probability of committing a Type II error means one can reject the Null. Rejecting the F-statistic Null hypothesis in this research means there is some relationship between at least one of the brightness temperatures and the synoptic temperature observation. Failing to reject the Null means that there is no relationship whatsoever between brightness temperature and synoptic temperature observation.

Finally, the t statistic examines the null hypothesis that the true regression equation of one data set is identical to that of another data set (Wilks, 1995). In the case of this research, it will test the Null Hypothesis

$$H_0 : \beta_{indicator} = 0 \quad (19)$$

against the Alternative Hypothesis

$$H_a : \beta_{indicator} \neq 0 \quad (20)$$

In other words, rejecting the t-statistic Null Hypothesis means there is a statistically significant difference between the true regression equations of the F10/F13 data and the F14 data. Failing to reject the Null indicates there is no such difference between the true regression equations of the F10/F13 data and the F14 data.

The software program S plus tests these hypotheses using the t statistic, t^* . The criterion for rejecting the null for a rejection level of .01 is

$$|t^*| \geq t_{.005, n-(k+1)} \quad (21)$$

The critical value of $t_{.005, n-(k+1)}$ could be found in a statistical table if it was necessary, but a computer makes this calculation much more quickly. For example, Figure 10 shows the critical values for a t statistic where $n = 100$ and $k = 7$, (i.e. there are 92 degrees of freedom).

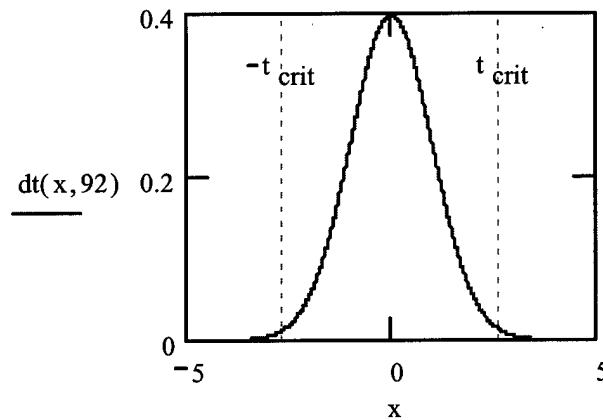


Figure 10: critical values $|t^*| > t_{.005, 92}$

As was the case with the F statistic, the number of degrees of freedom will change with each data set. Thus, instead of carrying different critical values through the results, I will instead show the "P-value." The only difference between the P-value for the F statistic and the P-value for the t statistic is that, because we are performing a 2-sided test of the Null, our critical P-value is .005 instead of .01.

Summary

A four phase process was used to gather matched data sets, sort them by season and land type, and combine the data used by Harris (1998) and Comoglio (1997) from Fall 1996 with new data from the F14 satellite from Fall 1997. Four statistics were used to analyze the data: RMSE, R squared, the F statistic, and the t statistic. With all of the groundwork now laid, analysis of the results can begin.

IV. Results Analysis

Chapter Overview

The results of the research were mixed. After outlining the statistics calculated to cross-validate data from different satellites, a possible explanation for the results will be offered. The data was then split and cross-validated. A comparison was done between the cross-validated root mean squared predictor error values and Harris's root mean squared error values using the old CV coefficients.

Data Sets

The data was sorted by season and land type. The bulk of data analysis was done using F10/F13 data from October 1996 and F14 data from September 1997. Since there was no F14 data to coincide seasonally with Jan/Feb 1997 data, and since some of the CONUS data from August 1996 was unreadable, these data sets were not used in the main research. However, some non-validated multiple linear regression was performed on these data sets; the results of these are in Appendix A.

Qualitative Regression Results

After the indicator variable was added to the data as described in Chapter III, stepwise linear regressions were performed upon the data (not including the indicator variable) to determine which of the brightness temperature channels were statistically significant in calculating surface temperature. After stepwise linear regression was used to eliminate the channel temperatures that did not significantly contribute to the regression, a second multiple linear regression was performed, including the indicator

variable, to determine if satellite identity was a significant factor in the regression.

Following are the results of this qualitative regression:

Table 4. Results of Qualitative Regression
Null Hypothesis: Satellite Identity is not significant in regression
Critical P-Value for Rejection of Null: 0.01

Land Type	# of Data Sets	T Statistic	P Value	Null Rejected
Dry, Arable Soil	681	-2.34	0.0196	No
Moist Soil	346	0.3688	0.7125	No
Semidesert	48	3.514	0.0007	Yes
Desert	305	2.05	0.0408	No
Dense Vegetation	83	0.8341	0.4068	No
Mixed Water/Vegetation	0	N/A	N/A	N/A
Light Vegetation	740	1.2467	0.2129	No
Wet Soil	205	5.261	0	Yes
Indeterminate Land Type	1292	14.0974	0	Yes

To summarize the results above, the satellite from which the data was gathered does not appear to impact the regression significantly in the cases of dry soil, desert, dense vegetation, light vegetation, and moist soil land types. The satellite identity does appear to have a significant impact upon the regression coefficients of the wet soil, semidesert and indeterminate land types.

Discussion

Note the extreme disparity between the t statistics for the calculated land types compared to indeterminate land types. The t statistics for the calculated land types did not exceed 5.261, while the t statistic for the miscellaneous category was a rather large 14.0974. From this, it would appear the correlation between satellite identity and regression coefficients is far less pronounced when the CV algorithm can determine a land type. The most plausible explanation is that the earth locations that registered as

“indeterminate” land types changed between the F10/F13 and F14 data sets. Because the data is from different years, it is possible the weather was significantly different at some locations. The land type algorithms are especially sensitive to heavy rainfall (McFarland, 1991); a heavy rain event one year but not the other could send a large number of data points into the “indeterminate” category.

Significant differences between the F10/F13 and F14 data sets might also explain the rejection of the Null Hypothesis for the Wet Soil and Semidesert land types.

Unfortunately, due to data constraints, the two data sets come from subsequent years – and not even exactly the same time of year. Differences in precipitation, soil moisture, and even evaporation rates can cause changes in surface radiation fluxes (Betts and Ball, 1998). Therefore, it is entirely possible that the statistical differences found in the data sets for the two recalcitrant land types were due to factors other than satellite identity. The significant finding of this research is that, despite other possible significant differences between data sets, the Null Hypothesis was NOT rejected. In other words, rejection of the Null Hypothesis for the Semidesert and Wet Soil land types merely indicates there was a statistically significant difference between the two data sets; it was not determined if this difference is due to satellite identity or other intrinsic differences in the data set.

Regression Coefficient Refinement

For the five land types whose regression coefficients do not appear to be affected by satellite identity, multiple linear regression on all of the data from the F10, F13 and F14 satellites was performed. Following are the results of the regression. The regression results, scatter plots and coefficients are in the tables and diagrams below. The scatter

plots in figures 11-15 are "45 degree" plots of the actual temperature versus the temperature value calculated by the regression.

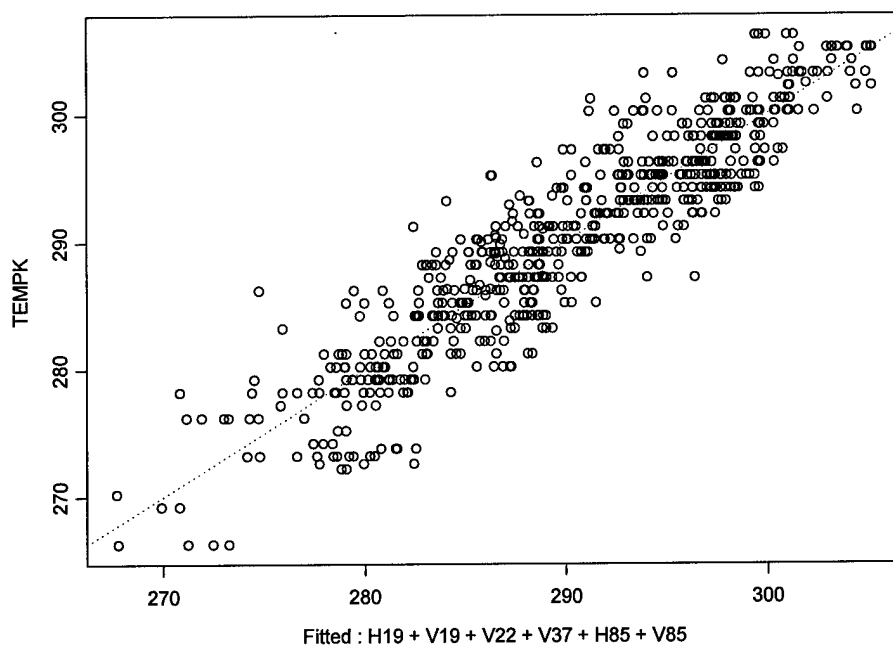


Figure 11: Scatter Plot for Dry Soil Land Type
 Regression Equation: $T_{fit} = 25.8771 + 0.2307 H19 - 0.4528 V19 + 0.4578 V22 + 0.4385 V37 - 0.4624 H85 + 0.7436 V85$

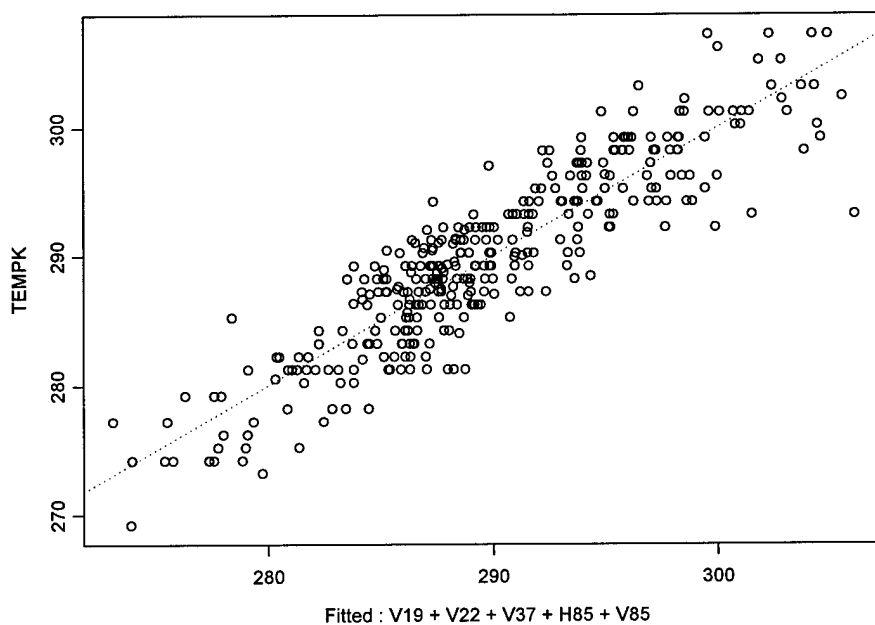


Figure 12: Scatter Plot for Moist Soil Land Type
 Regression Equation: $T_{fit} = 18.9090 - 0.3197 V19 + 0.6129 V22 + 0.4926 V37 - 0.8541 H85 + 1.0402 V85$

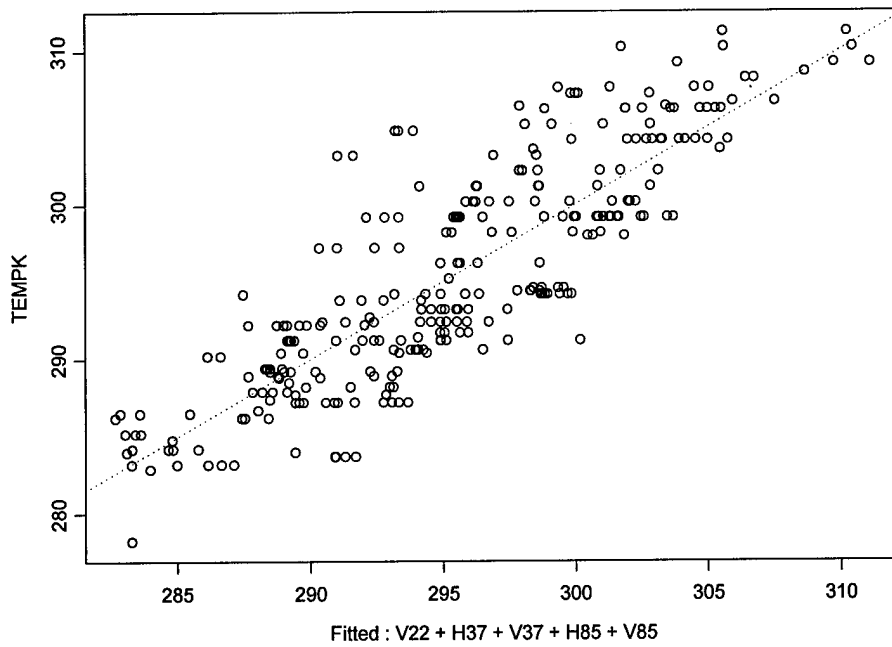


Figure 13: Scatter Plot for Desert Land Type
 Regression Equation: $T_{fit} = 32.5467 + 0.5766 V22 - 1.0011 V37 - 0.2832 H85 + 1.1725 V85$

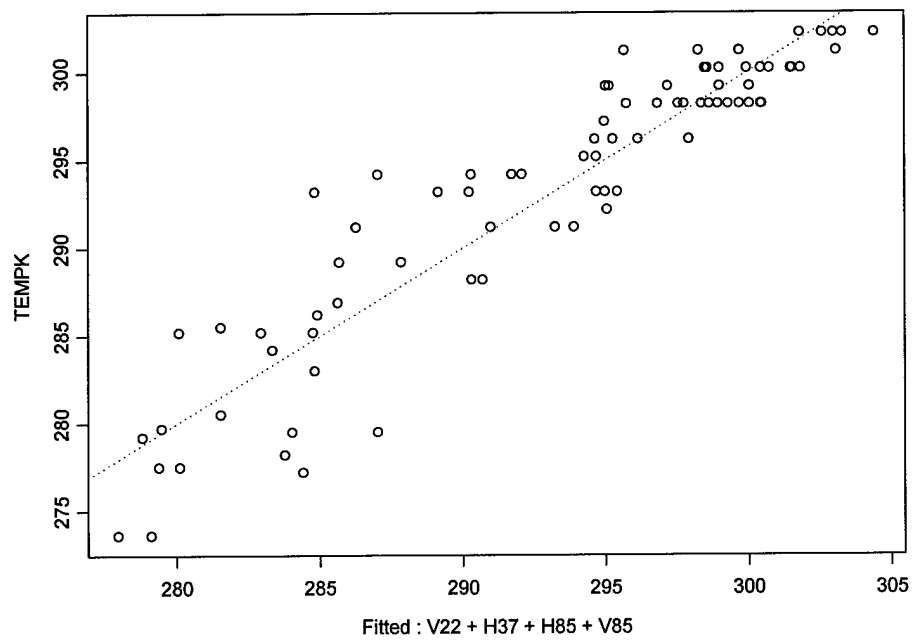


Figure 14: Scatter Plot for Dense Vegetation Land Type
 Regression Equation: $T_{fit} = (-14.5311) + 0.7351 V22 + 0.6965 H37 - 1.601 H85 + 0.8194 V85$

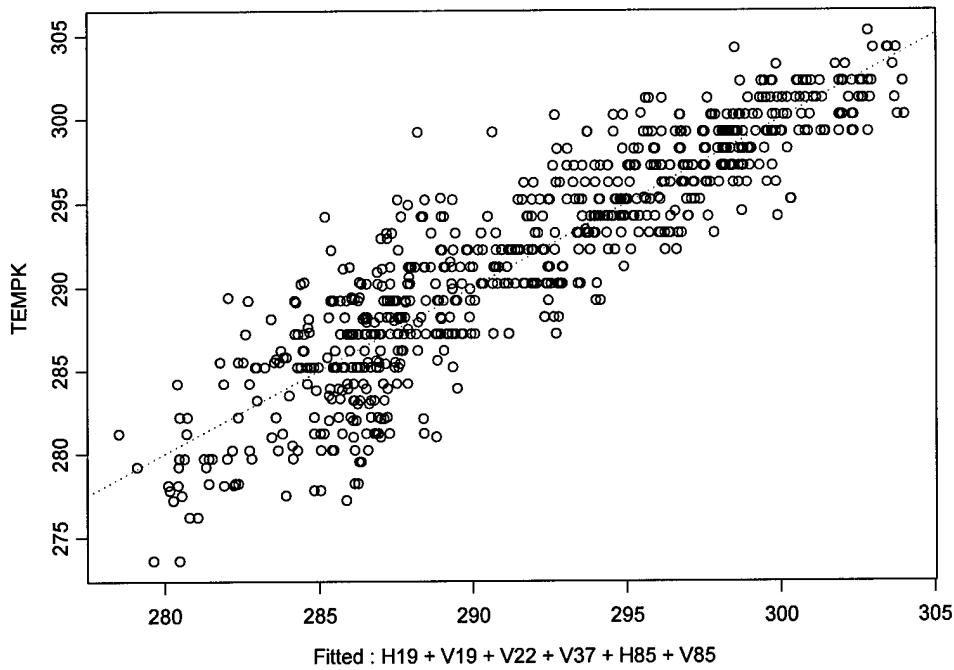


Figure 15: Scatter Plot for Light Vegetation Land Type
 Regression Equation: $T_{fit} = 24.0912 - 0.2110 H19 + 0.2663 V19 + 0.5340 V22 + 0.4725 V37 - 0.3786 H85 + 0.2688 V85$

Table 5. Combined Regression Results (All Satellites, F10/F13/F14)
 Null Hypothesis: All regression coefficients = 0

Land Type	# of Data Sets	F Statistic	P Value	Null Rejected	RMSE(K)	R squared
Dry, Arable Soil	681	590.4	0	Yes	3.301	0.8402
Moist Soil	346	293.1	0	Yes	3.089	0.8117
Desert	305	161.3	0	Yes	3.743	0.7295
Dense Vegetation	83	121.1	0	Yes	3.053	0.8613
Light Vegetation	740	557.4	0	Yes	2.825	0.8202

It is certainly noteworthy that the R squared values are quite high. Somewhat surprising is that the highest R squared value comes from the dense vegetation land type, the category with the smallest sample size. Following is a table that compares the calculated RMSE values of this research to the RMSE values in McFarland's original research.

Table 6: RMSE (K) Comparison to Original CV Regression

Land Type	McFarland RMSE	Adair RMSE
Dry Soil	3.60*	3.301
Moist Soil	2.78**	3.089
Desert	3.60*	3.743
Dense Vegetation	3.45***	3.053
Light Vegetation	2.69	2.825

* Combined regression for Dry Soil, Semidesert and Desert Land Types

** Combined regression for Moist Soil and Wet Soil Land Types

*** Combined regression for Dense Vegetation and Mixed Water/Vegetation Land Types

Cross-validation of the data sets

It is important to note the above regressions are for qualitative judgement only. The overall data sets were not split into training and validation sets – rather, the rejection of the Null Hypothesis in the indicator variable regression (see Table 4) was used as evidence the F10/F13 data and the F14 data for the five land types had identical true regression equations. However, to justify further the value CV coefficient refinement, the data was split and cross-validated. First, F10/F13 data from each land type was regressed; then, the coefficients were applied to the respective F14 data and MSPR values were calculated. Next, the reverse was done – F14 data was regressed and then the coefficients were used on the F10/F13 data for calculation of MSPR. Finally, the MSPR values were compared with the RMSE values found in Harris’s research. Following are the scatter plots of the cross-validations, followed by two tables summarizing the results.

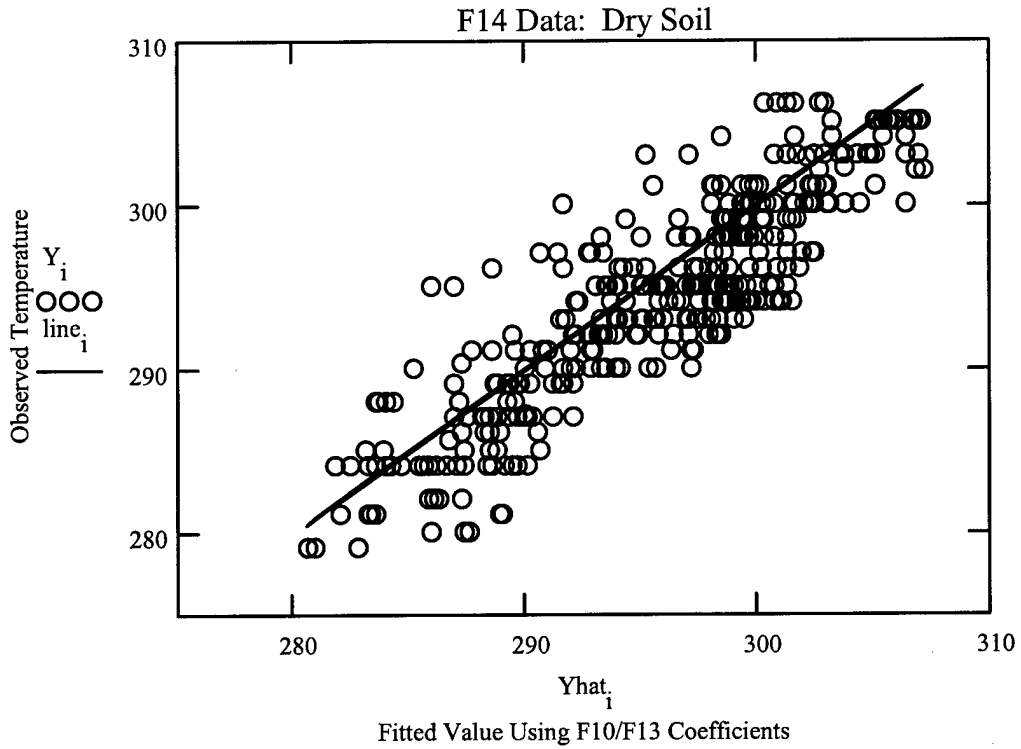


Figure 16: Cross validation of F10/F13 Coefficients on F14 data – Dry Soil
 $T_{fit} = 5.9964 + .3984 H19 - .7341 V19 + .5234 V22 + .6422 V37 - .5116 H85 + .7169 V85$

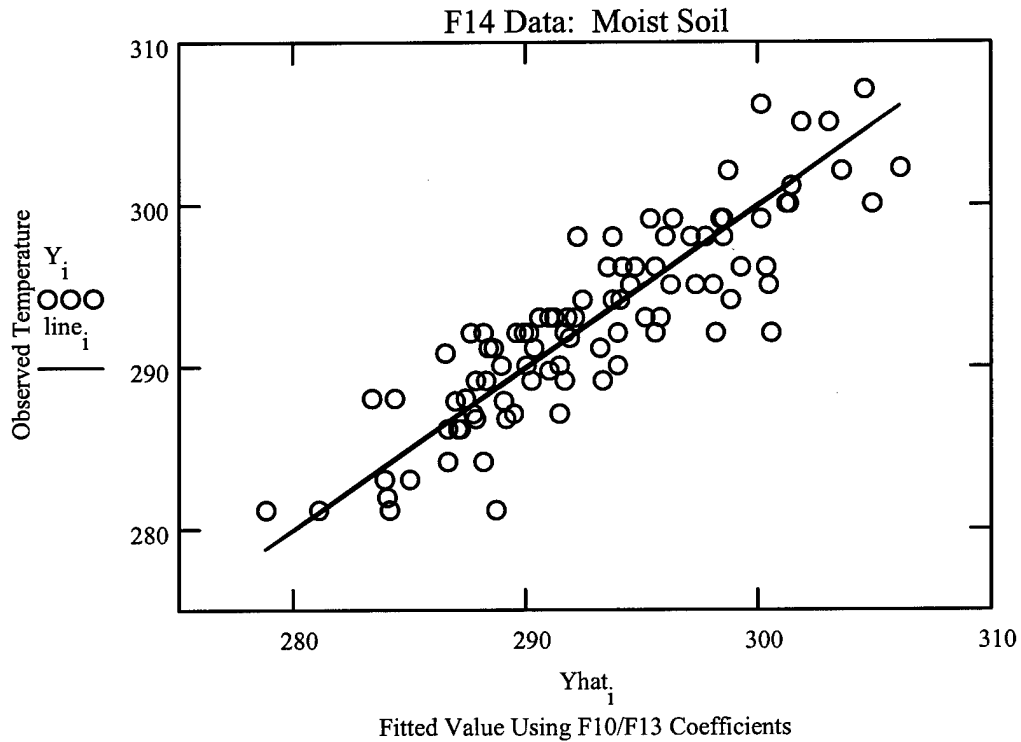


Figure 17: Cross-Validation of F10/F13 Coefficients on F14 Data – Moist Soil
 $T_{fit} = 13.1295 - .463 V19 + .7297 V22 + .776 V37 - .9434 H85 + .8936 V85$

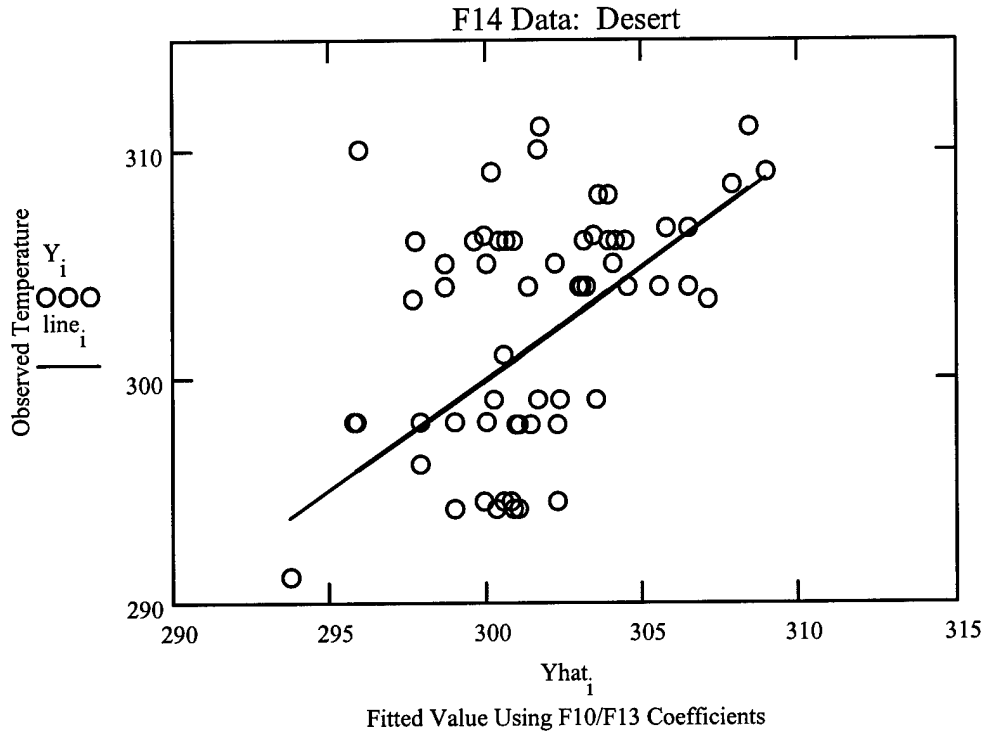


Figure 18: Cross-Validation of F10/F13 Coefficients on F14 Data – Desert
 $T_{fit} = 42.0952 - .398 V19 + .8684 V22 + .8167 H37 - 1.2924 V37 - .5523 H85$

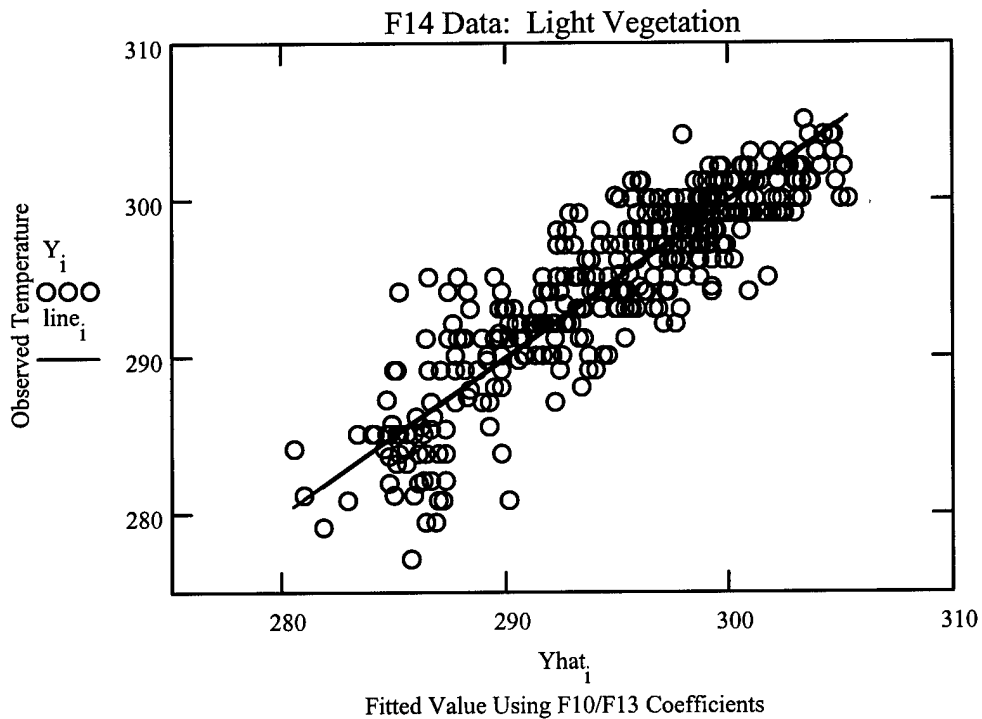


Figure 19: Cross -Validation of F10/F13 Coefficients on F14 Data – Light Vegetation
 $T_{fit} = 10.6856 - .584 H19 + .7251 V19 + .5375 V22 + .869 V37 - .5523 H85$

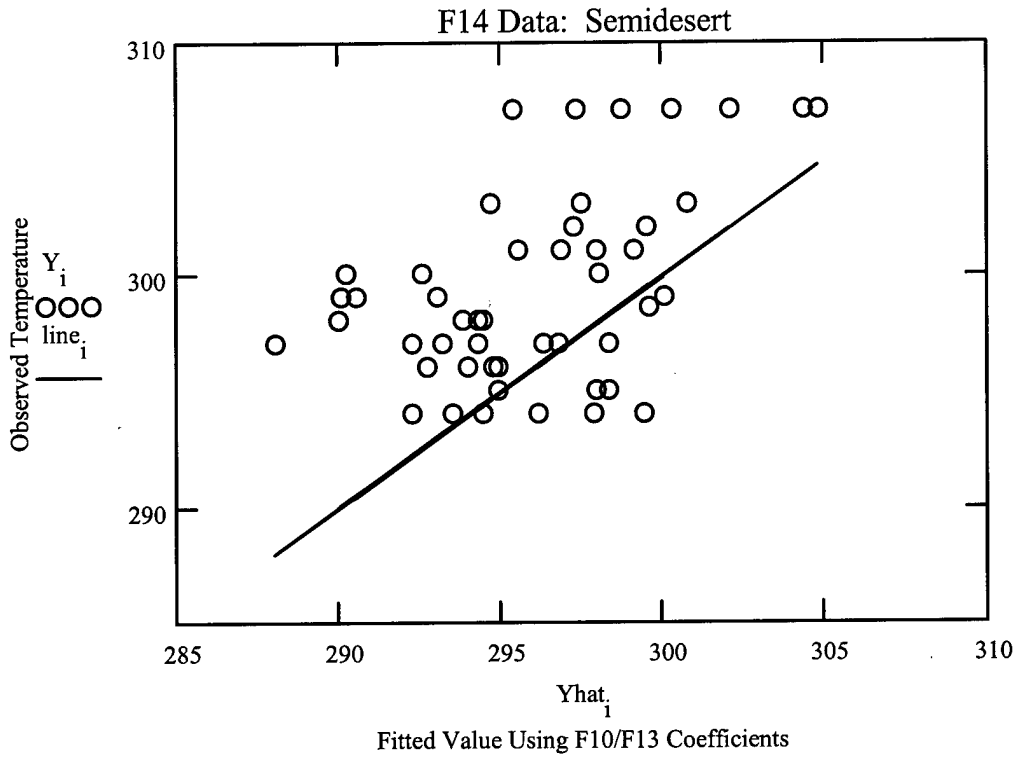


Figure 20: Cross-Validation of F10/F13 Coefficients on F14 Data—Semidesert (FAILED)

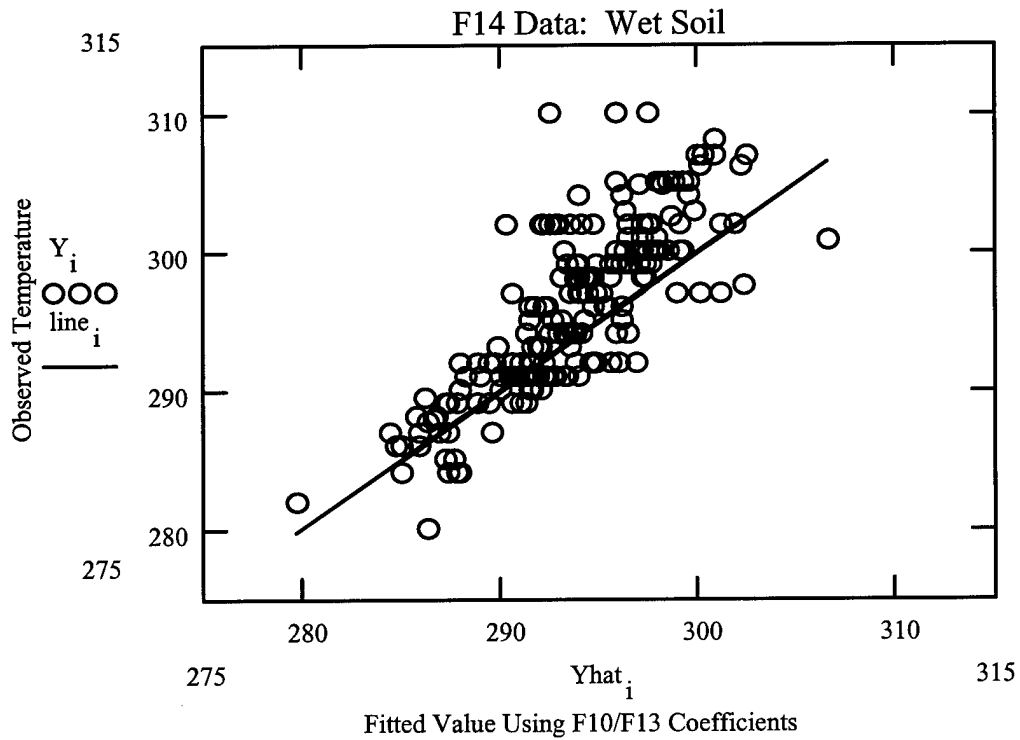


Figure 21: Cross-validation of F10/F13 Coefficients on F14 Data – Wet Soil (FAILED)

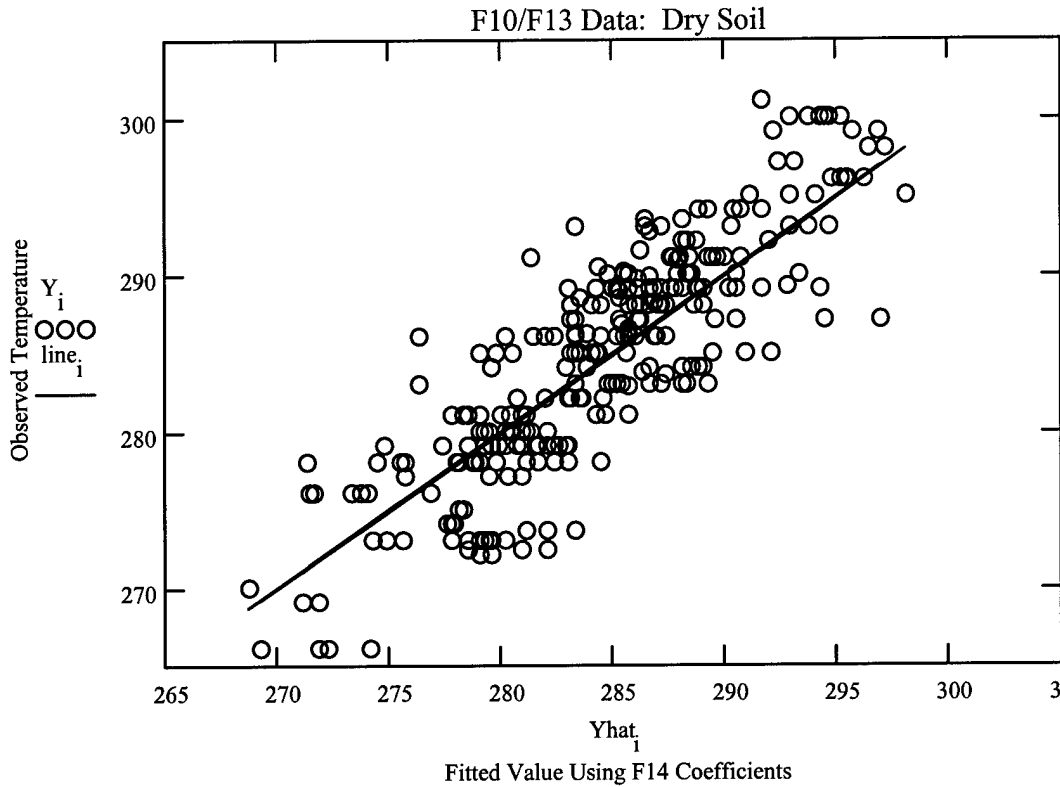


Figure 22: Cross-validation of F14 Coefficients Using F10/F13 Data – Dry Soil
 $T_{fit} = 33.4526 + .5575 V22 - .1941 H85 + .559 V85$

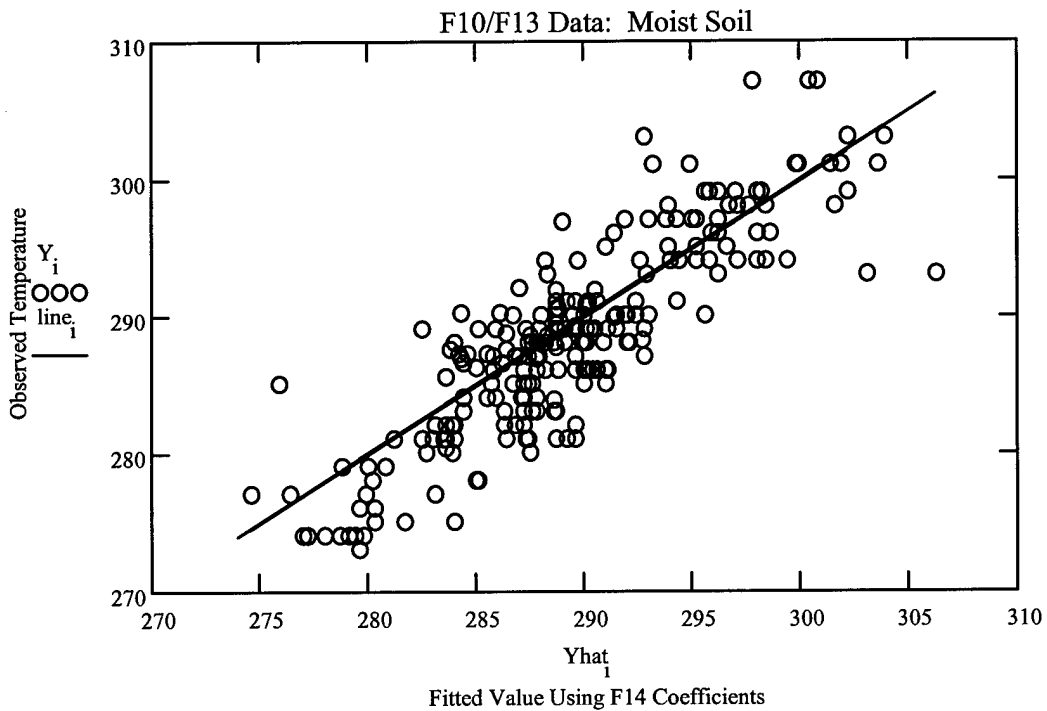


Figure 23: Cross-validation of F14 Coefficients Using F10/F13 Data – Moist soil
 $T_{fit} = 33.8725 + .5246 H37 - .9232 H85 + 1.3298 V85$

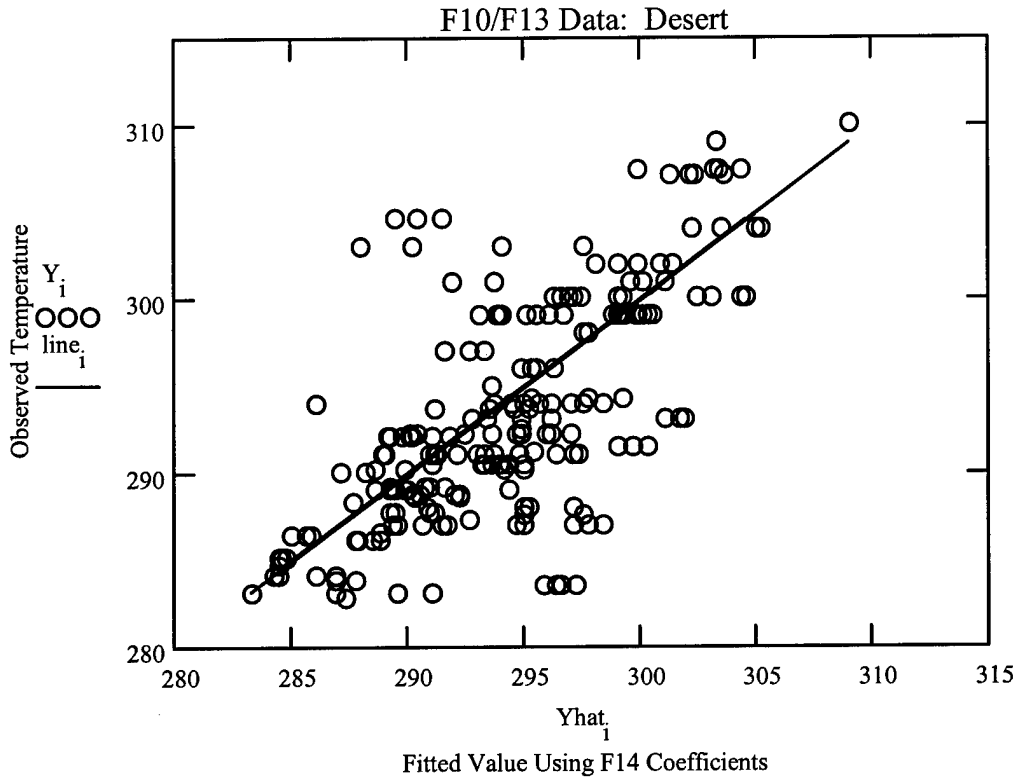


Figure 24: Cross-validation of F14 Coefficients Using F10/F13 Data – Desert
 $T_{fit} = 57.0802 + .6646 V22 + .1859 V85$

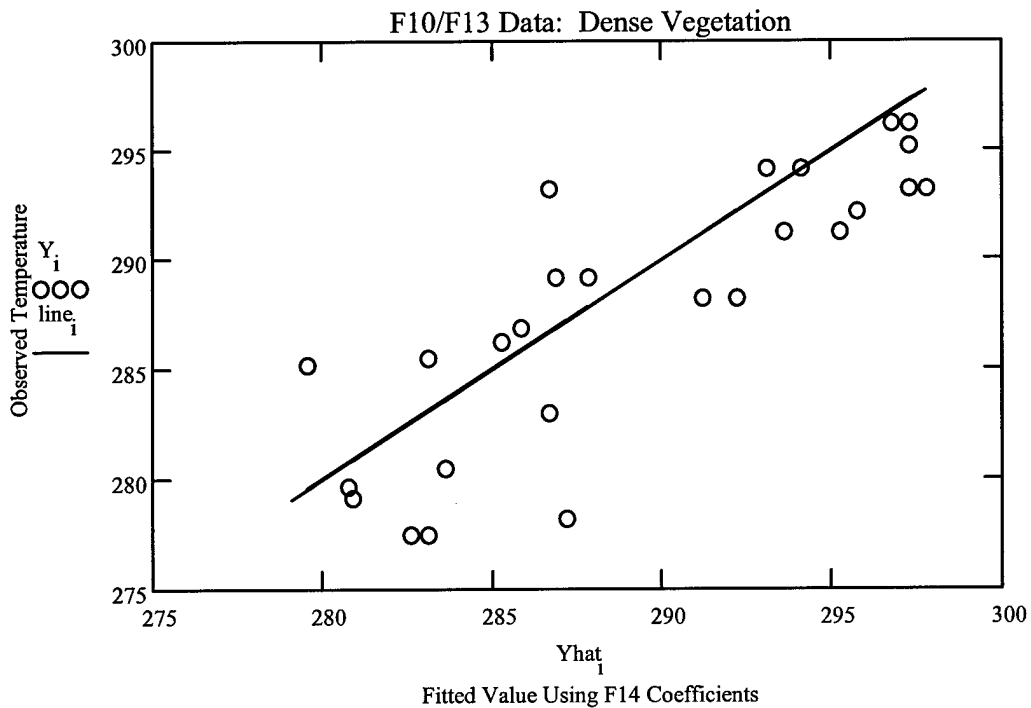


Figure 25: Cross-validation of F14 Coefficients using F10/F13 Data -- Dense Vegetation
 $T_{fit} = 8.2529 + .4995 H19 - 1.1686 H85 + 1.6808 V85$

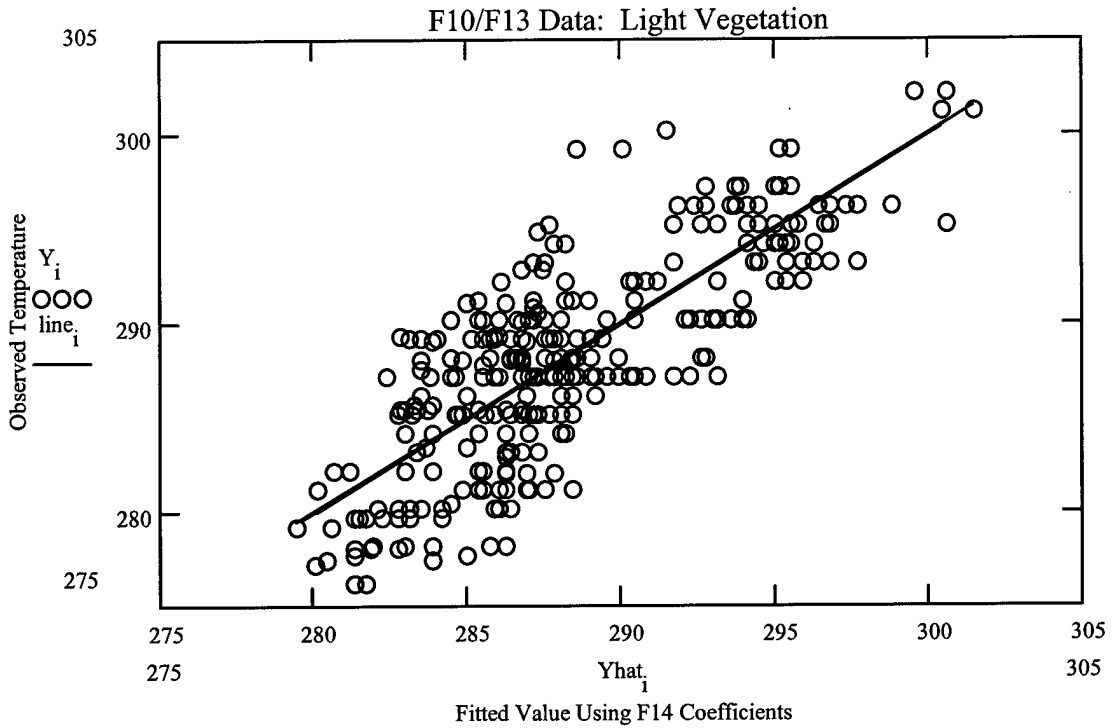


Figure 26: Cross-validation of F14 Coefficients Using F10/F13 Data – Light Vegetation
 $T_{fit} = 36.2198 + .5321 V22 + .3803 V85$

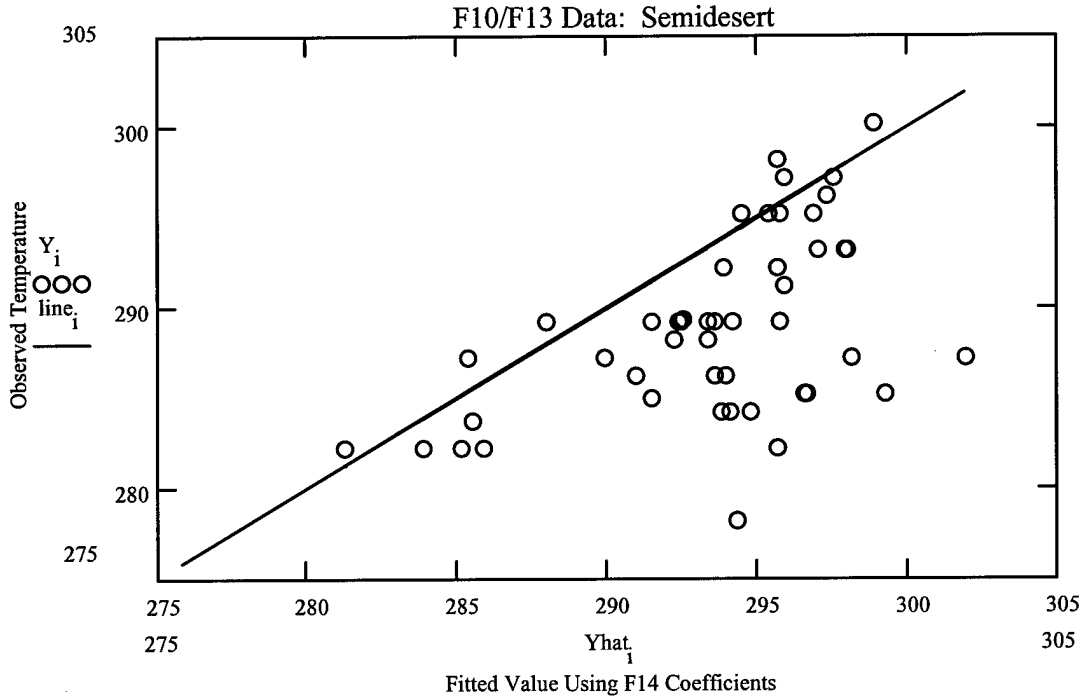


Figure 27: Cross-validation of F14 Coefficients Using F10/F13 Data – Semidesert
(F A I L E D)

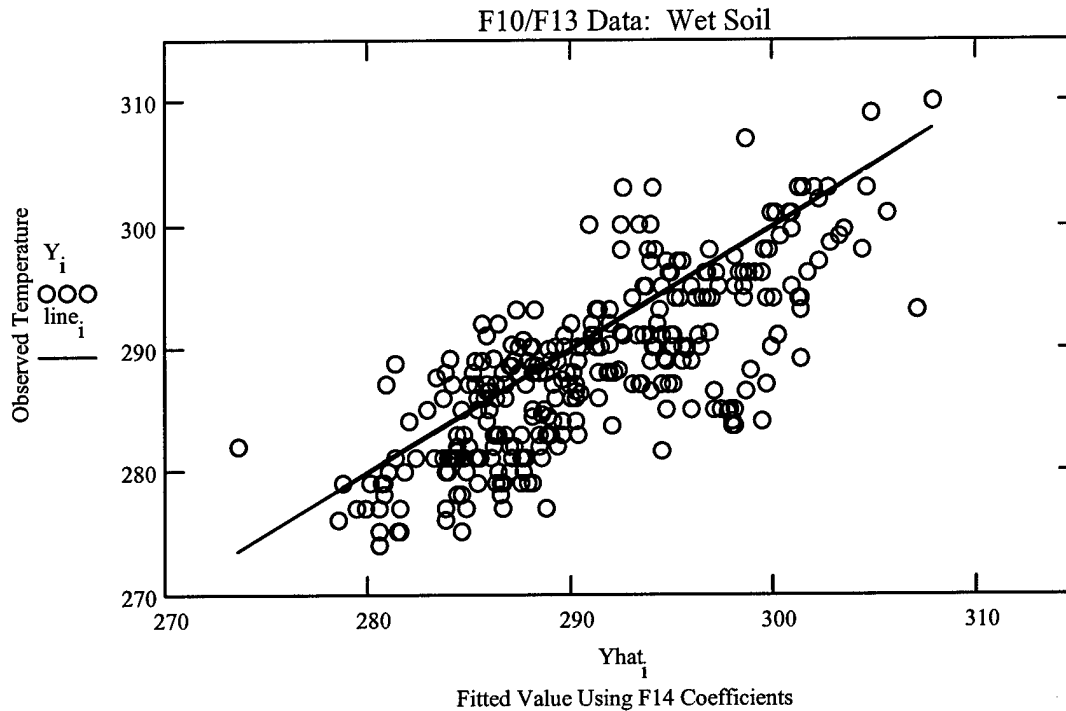


Figure 28: Cross-validation of F14 Coefficients Using F10/F13 Data – Wet Soil
(FAILED)

Table 7: RMSE and MSPR Values of F10/F13 Coefficients Cross-validated on F14 Data

Land Type	RMSE	RMSPR	R-Squared	Indicator Variable Test
Dry Soil	3.686	3.297	0.7499	Pass
Moist Soil	3.193	2.877	0.8033	Pass
Wet Soil	4.284	4.409	0.6254	Fail
Semidesert	3.326	5.221	0.7945	Fail
Desert	3.619	4.773	0.6791	Pass
Light Vegetation	3.128	2.687	0.6861	Pass

Table 8: RMSE and MSPR Values of F14 Coefficients Cross-validated on F10/F13 Data

Land Type	RMSE (K)	RMSPR (K)	R-Squared	Indicator Variable Test
Dry Soil	2.957	3.853	0.785	Pass
Moist Soil	2.534	3.708	0.8188	Pass
Wet Soil	3.547	5.174	0.665	Fail
Semidesert	2.993	7.072	0.516	Fail
Desert	2.891	4.746	0.6979	Pass
Light Vegetation	2.456	3.337	0.8227	Pass
Dense Vegetation	2.945	3.896	0.8062	Pass

The results of the cross-validation were quite encouraging. Even the RMSPR values of the land types that failed the indicator variable test were comparable with the RMSE values from Harris. The RMSPR values for the land types that passed the indicator variable test were lower than those RMSE values found by Harris.

Table 9: RMSE (K) of CV Algorithm from Harris (1998)
 (For comparison: Highest Validated RMSPR From Research: 4.8 K)

	Summer	Fall	Winter
CONUS	7.8	5.6	6.2
Bosnia	19.4	5.3	5.2
Korea	8	6.2	6.2
Saudi Arabia	7.4	7.4	7.4

From the above results, it is reasonable to conclude that a comprehensive linear regression to refine brightness temperature coefficients would yield more accurate results.

Perhaps most perplexing were the differing results by land type between the two data sets. If the F10/F13 and F14 data sets were insufficiently similar, it would follow that data for all land types would have shown statistically significant differences. Conversely, if the data sets were sufficiently similar, then all of the land types should have indicated so. This researcher speculates that the Wet Soil and Semidesert land types either (1) are more sensitive to changing weather between years than other land types, (2) are situated in locations prone to more radical weather changes than locations of other land types, or (3) have emissivity characteristics which are more location dependent than those for other land types.

Summary

Qualitative regression indicated satellite identity might not be a significant factor in determining the regression coefficients for five of eight CV land types. The same regression indicated satellite identity might be a significant factor for two land types, as well as for data of an indeterminate land type. The "Mixed Water and Vegetation" land type had no data ascribed to it, and so the regression for that land type could not be performed. Multiple linear regression was performed upon the five satellite-independent land types. Results indicated reasonable RMSEs and high R squared values. Cross-validation yielded MSPRs that compared favorably with RMSEs found from Harris's use of the original coefficients. Therefore, it appears CV could be made more accurate with revised coefficients.

V. Summary, Conclusions and Recommendations

Summary

Using the statistical methods of multiple linear regression, stepwise linear regression, and qualitative regression, 3,700 data sets from Fall of 1996 and Fall of 1997, including microwave brightness temperatures from three satellites, were analyzed to determine if satellite identity had a significant impact on CV regression coefficients. Analysis indicated that satellite identity does not appear to have a significant impact on the regression coefficients for five of the eight CV land types investigated. Analysis of two CV land types indicated satellite identity might have a significant impact, while there was insufficient data to determine the impact for one CV land type.

In addition to the qualitative regression, stepwise linear regression was performed on five land type categories using combined data from all satellites. Regressed RMSEs ranged from 2.825 K to 3.743 K, while R squared values ranged from .7295 to .8613. Preliminary analysis indicated refinement of CV brightness temperature coefficients may yield better accuracy for the algorithm.

Finally, the data was cross-validated by splitting the data, regressing each set, and calculating the MSPRs when the regressed coefficients were used on the other data set. The results of the cross-validation confirmed the results of the indicator variable regression.

Conclusion and Recommendation for AFWA

The assumption that CV coefficients need not be recalculated for each satellite appears sound for most of the data. However, satellite identity might have a significant impact upon the regression for at least two of the land types. Therefore, AFWA should consider further testing the algorithms for the semidesert and wet soil land types to see if there is indeed satellite dependence for these two land types. Because of unique properties of “indeterminate” land type data as discussed in Chapter 4, AFWA should investigate regressing location and rainfall dependent coefficients for data which the CV algorithm cannot determine a land type.

Recommendations for Further Research

The first research project I recommend would be to investigate the characteristics of the Semidesert and Wet Soil land types. While it is possible these two land types are satellite dependent for some reason, it is more likely that the data needs to be split into other categories. For example, it is possible the data needs to be split depending on the seasonal amount of rainfall received. Perhaps the differences would be ameliorated if a larger data set were used to include more varied cases. Finally, the land types could be split by the amount of rainfall received in a given period of time – for example, the previous 12 hours.

The first part of the above project, determination of satellite dependence, would be relatively straightforward. A large number of data sets from identical areas of known semidesert and wet soil land types (that is, land types known beforehand rather than determined by the CV algorithm) and near-identical times could be calculated using

different DMSP satellites. Qualitative regression could then be performed as was done in this research. If the statistics still show a significant difference between the data sets, then sensor dependence can be shown.

Assuming no sensor dependence, the second part of the project would be considerably more involved. SSM/I brightness temperatures would need to be correlated not just with observed temperature, but also with current precipitation intensity, precipitation amounts for a given time in the past, and climatological precipitation data by location and season. The current precipitation intensity could be calculated using SSM/I rain rate algorithms (e.g. Ferraro et al., 1998), but determining and correlating the latter two parameters would be a time-intensive and data sparse process.

Another avenue of follow-on research would be to modify the CV algorithm's coefficients and improve its accuracy. All available DMSP data should be combined with synoptic observations to create an enormous database. FORTRAN programs could then be written to match data, separate data into land types, and separate data by satellite identity. Data could be combined and regressed for five of the land types, while separate regressions by either satellite, precipitation intensity or location could be accomplished for the semidesert and wet soil land types. Finally, a single FORTRAN program could be constructed to accomplish all of the above tasks and incorporate the calculated coefficients.

Another possible use of indicator variables is to determine if the location of observations (e.g., CONUS versus Middle East) has an impact on the regression coefficients (see Ferraro et al., 1998). This research did not divide the data by location because there was insufficient data in some locations and/or land types to perform a

comprehensive study. A study could be done performing qualitative regression on an indicator variable for two different regions.

Another avenue for further research would be to examine the effects of precipitation upon the regression coefficients. An indicator variable could be constructed to represent precipitation intensity and then regressed, using a multiple value indicator variable instead of a Bernoulli indicator variable (see Chapter 10 of Neter et al., 1983). Depending upon the results, an SSM/I rain-rate retrieval algorithm (see Conner and Petty, 1998) could be incorporated into CV to refine temperature calculation further.

This research did not address the possibility of errors introduced by the surface type algorithms themselves. A possible topic of future research would be to examine the locations of the data matches sorted into various land types. A map outlining locations and categories of various land type matches could be generated to see if such land types exist. For example, if there were a number of "moist soil" land type hits in the middle of the Sahara Desert, or a number of "desert" hits in the Amazon, it would indicate the land type sorting algorithms are in error.

Finally, research could be performed to determine if a polynomial regression would fit the data better. However, while the regression indicated slight deviation from normality at extremely high and low temperatures (see Appendix B), the high R squared values suggest research time might be spent first on the research topics outlined above.

Appendix A: Other Regression Performed but Not Directly Used in the Research

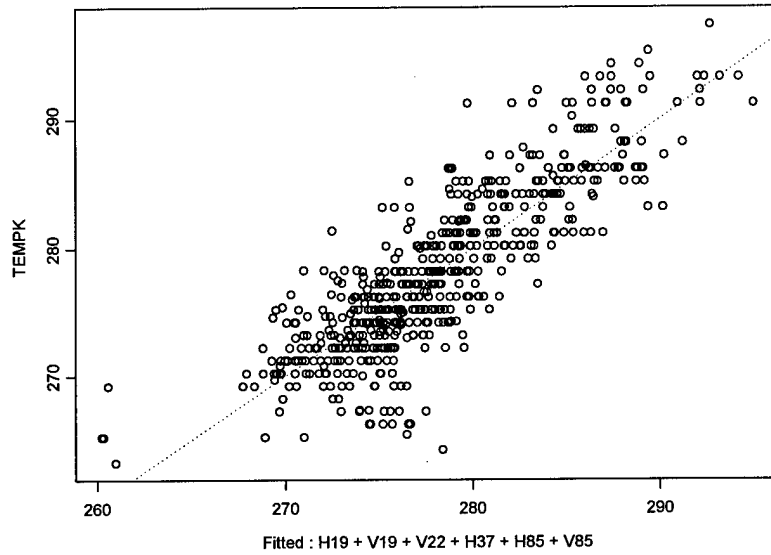


Figure A1: Scatter Plot for Dry Soil Land Type, Jan-Feb 1997, F10/F13
Regression Equation: $T_{fit} = 8.0986 - 0.1447 H19 - 0.2169 V19 + 1.0707 V22 + 0.2780 H37 - 0.2762 H85 + 0.3041 V85$

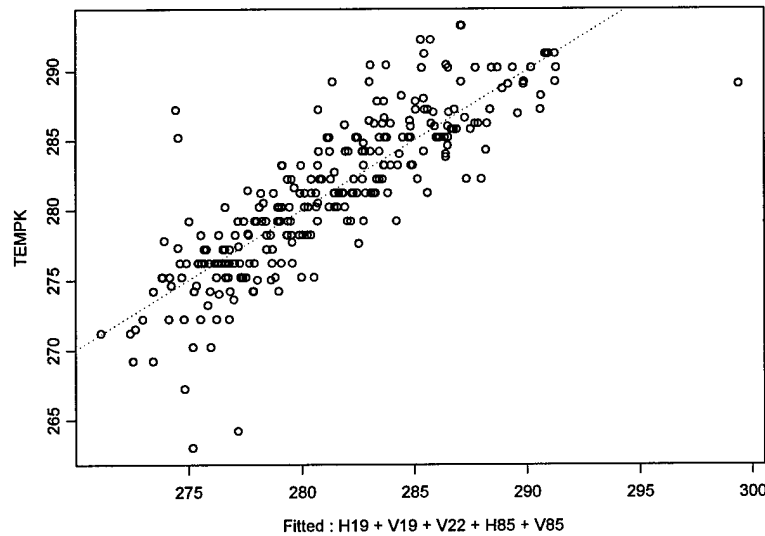


Figure A2: Scatter Plot for Moist Soil Land Type, Jan-Feb 1997, F10/F13
Regression Equation: $T_{fit} = 21.1260 - 0.3748 H19 + 0.3105 V19 + 0.5380 V22 - 0.4812 H85 + 0.9579 V85$

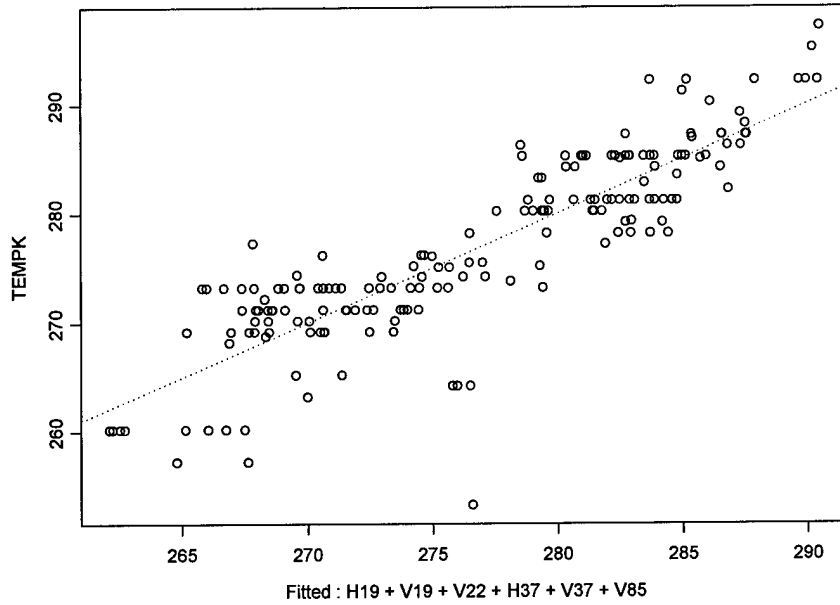


Figure A3: Scatter Plot for Semidesert Land Type, Jan-Feb 1997, F10/F13
 Regression Equation: $T_{fit} = 88.4597 - 0.6082 H19 + 0.5872 V19 + 1.1129 V22 + 0.3985 H37 - 1.1530 V37 + 0.3645 V85$

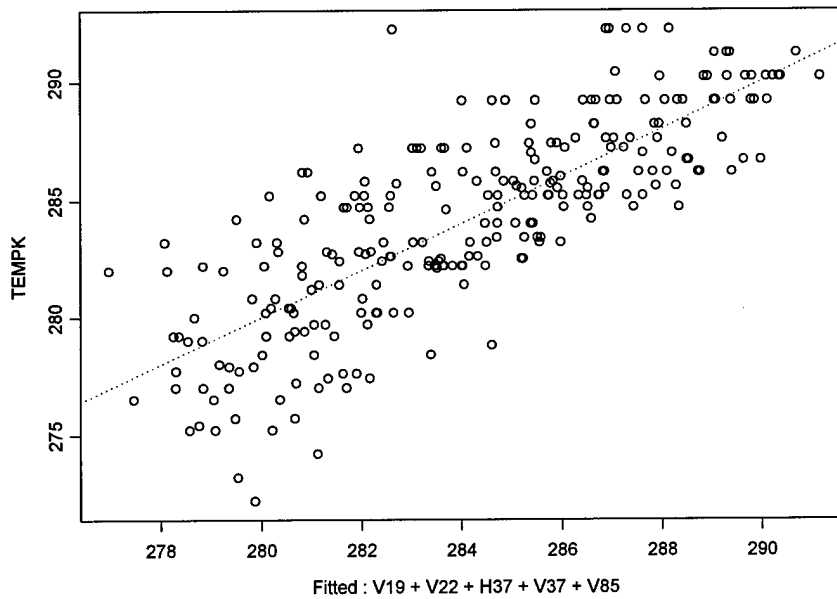


Figure A4: Scatter Plot for Desert Land Type, Jan-Feb 1997, F10/F13
 Regression Equation: $T_{fit} = 94.7734 + 0.4267 V19 + 0.3087 V22 + 0.2945 H37 - 0.7946 V37 + 0.4776 V85$

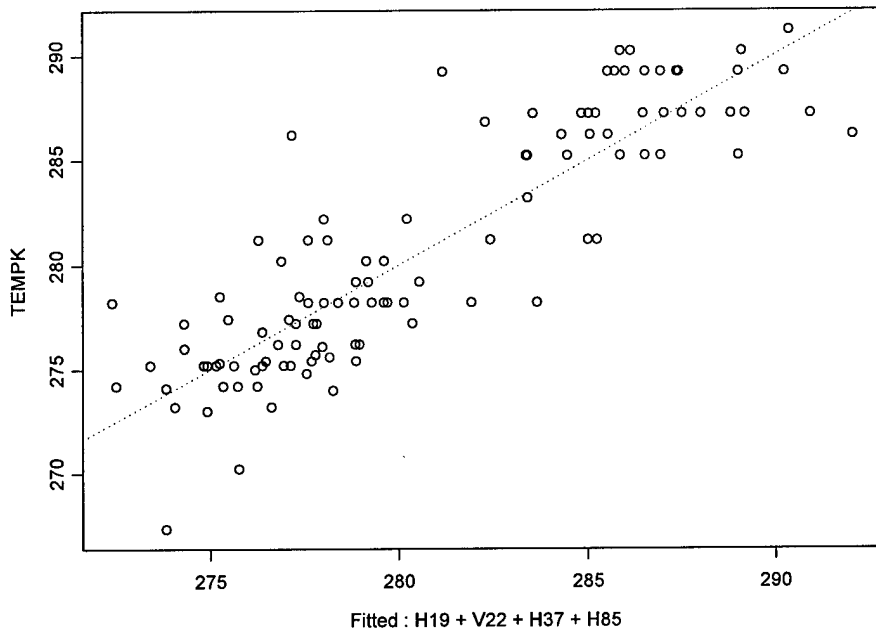


Figure A5: Scatter Plot for Light Vegetation Land Type, Jan-Feb 1997, F10/F13
 Regression Equation: $T_{fit} = (-44.3633) + 0.5181 H19 + 0.7982 V22 + 0.8012 H37 - 0.8961 H85$

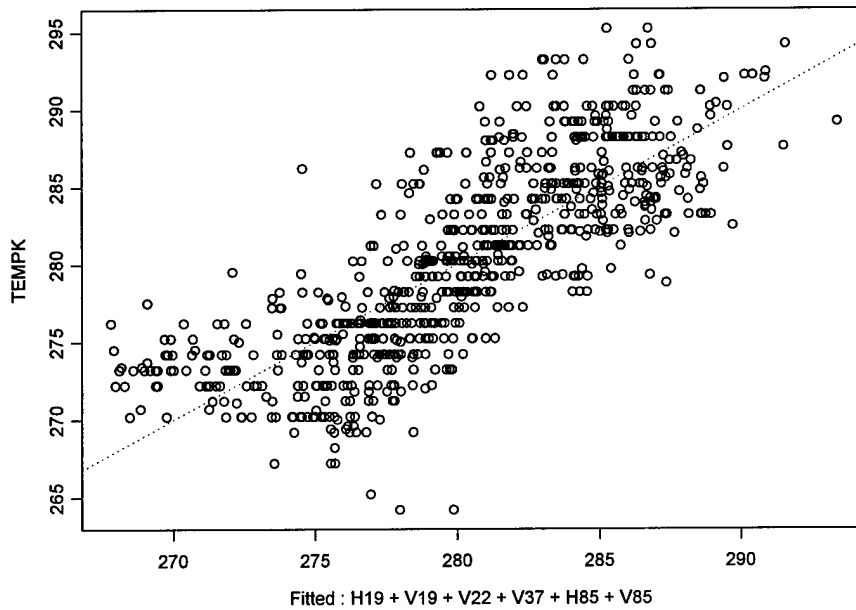


Figure A6: Scatter Plot for Wet Soil Land Type, Jan-Feb 1997, F10/F13
 Regression Equation: $T_{fit} = 137.6667 - 0.2642 H19 + 0.3931 V19 + 0.3170 V22 - 0.3191 V37 - 0.1080 H85 + 0.5019 V85$

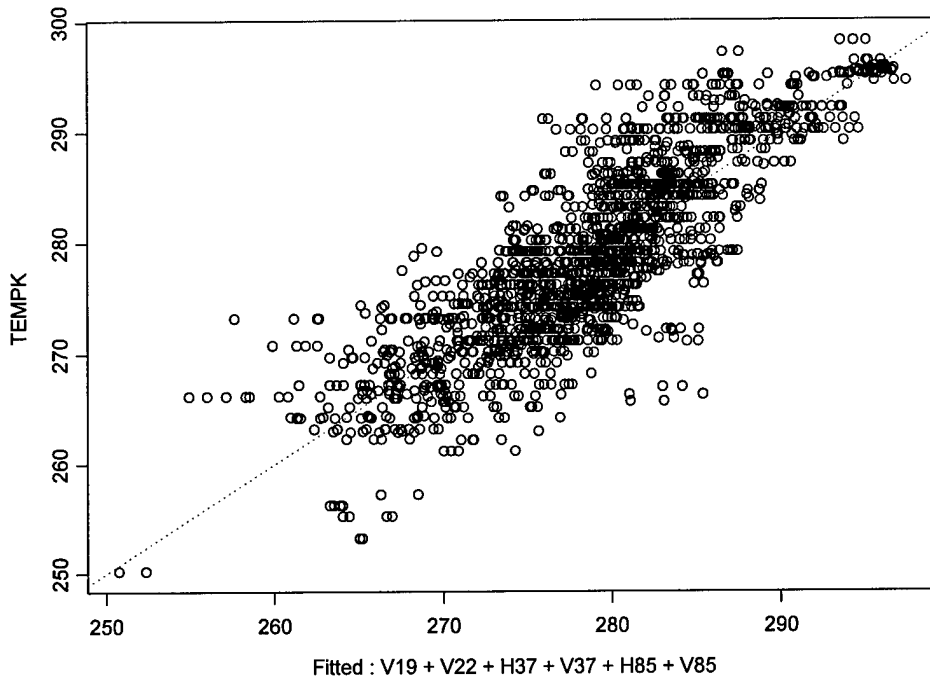


Figure A7: Scatter Plot for Indeterminate Land Type, Jan-Feb 1997, F10/F13
 Regression Equation: $T_{fit} = 161.3059 - 0.2227 V19 + 0.4300 V22 - 0.1430 H37 + 0.0614 V37 - 0.1225 H85 + 0.4366 V85$

Table A1: Regression Results (F10/F13) for Jan-Feb 1997
 Null Hypothesis: All regression coefficients = 0

Land Type	# of Data Sets	F Statistic	P Value	Null Rejected	RMSE(K)	R squared
Dry, Arable Soil	579	247.8	0	Yes	3.413	0.7222
Moist Soil	283	141.8	0	Yes	2.981	0.719
Semidesert	184	88.3	0	Yes	4.214	0.7496
Desert	259	88.8	0	Yes	2.553	0.6369
Dense Vegetation	0	N/A	N/A	N/A	N/A	N/A
Mixed Water/Veg	0	N/A	N/A	N/A	N/A	N/A
Light Vegetation	112	89.1	0	Yes	2.773	0.7691
Wet Soil	758	208.8	0	Yes	3.831	0.6252
Indeterminate	1881	725.3	0	Yes	4.581	0.699

Appendix B: Residual and Normality Plots of the F10/F13/F14 Regression

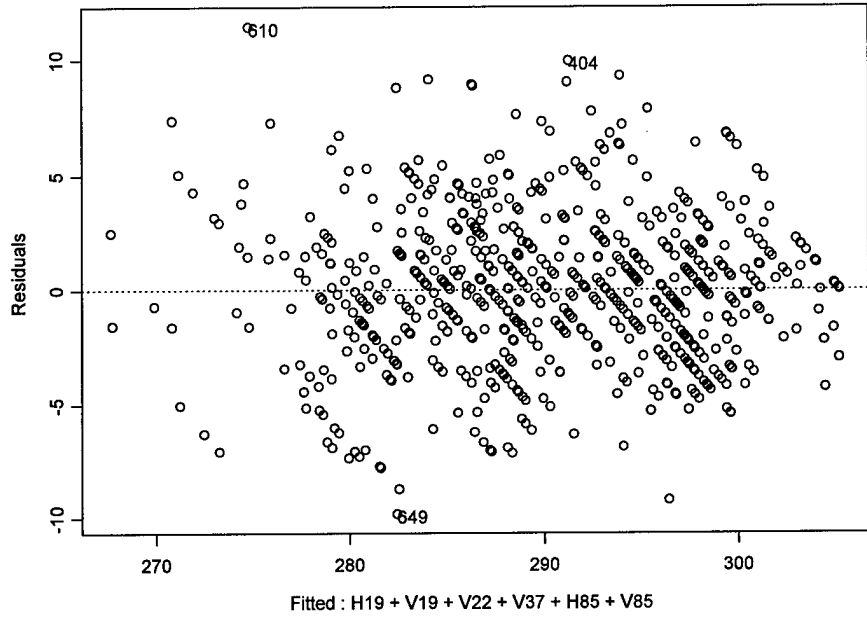


Figure B1: Residual Plot for Dry Soil Land Type

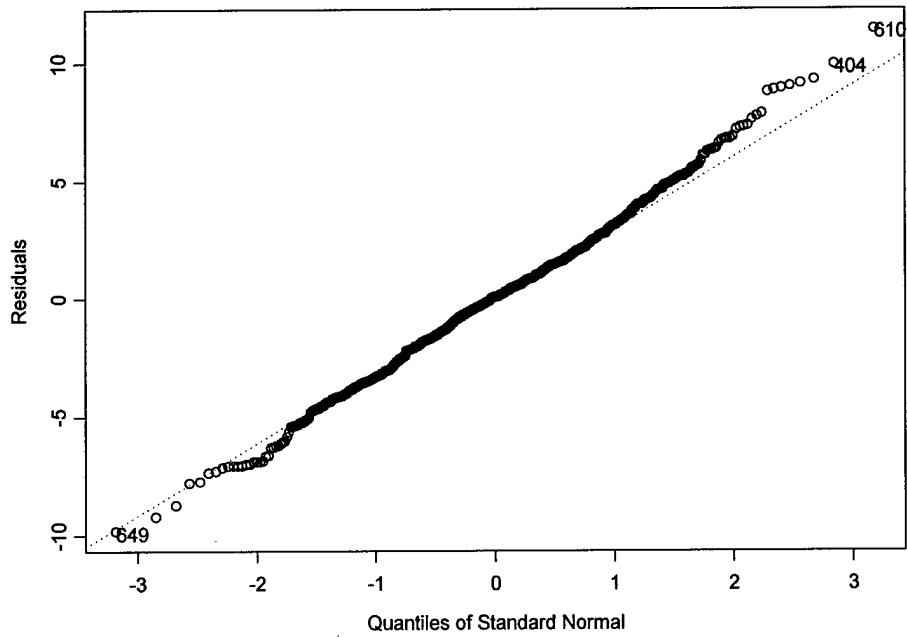


Figure B2: Normality Plot for Dry Soil Land Type

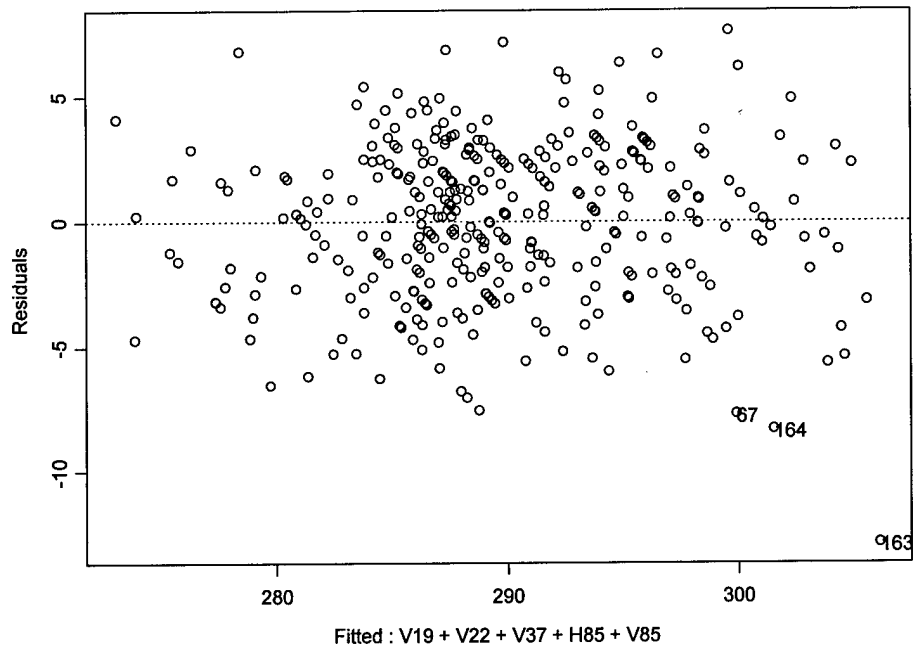


Figure B3: Residual Plot for Moist Soil Land Type

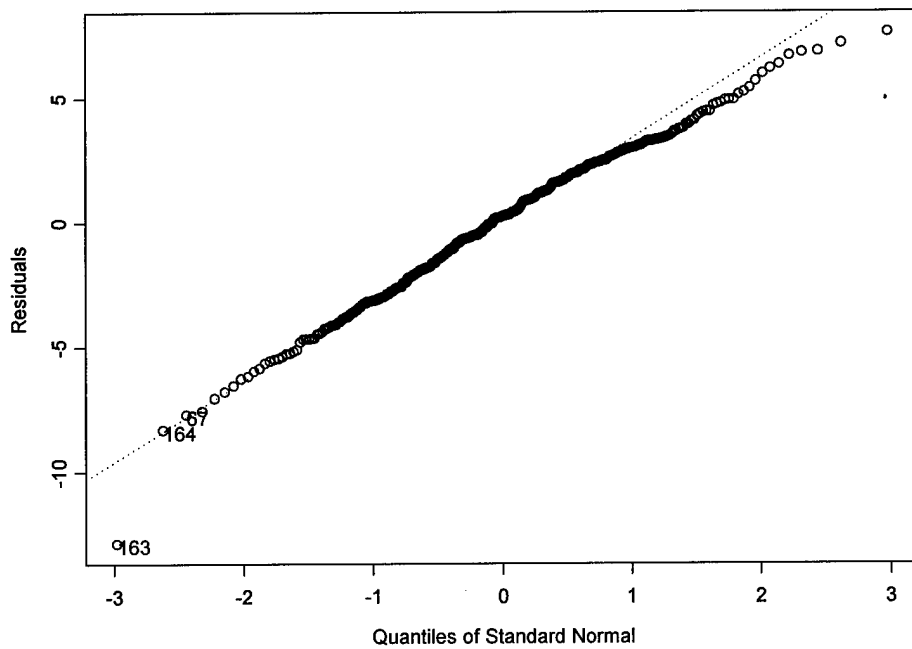


Figure B4: Normality Plot for Moist Soil Land Type

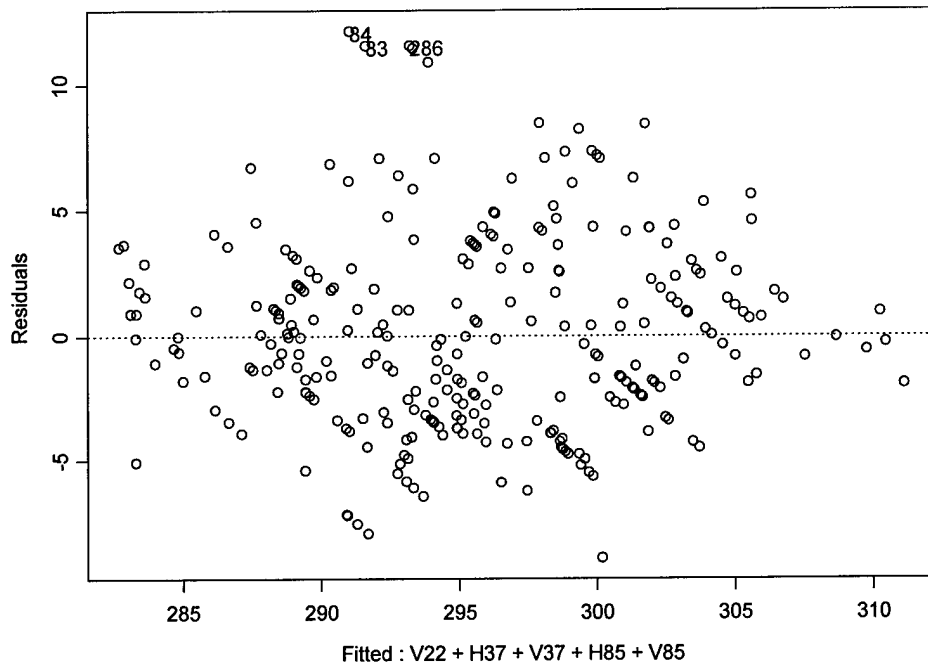


Figure B5: Residual Plot for Desert Land Type

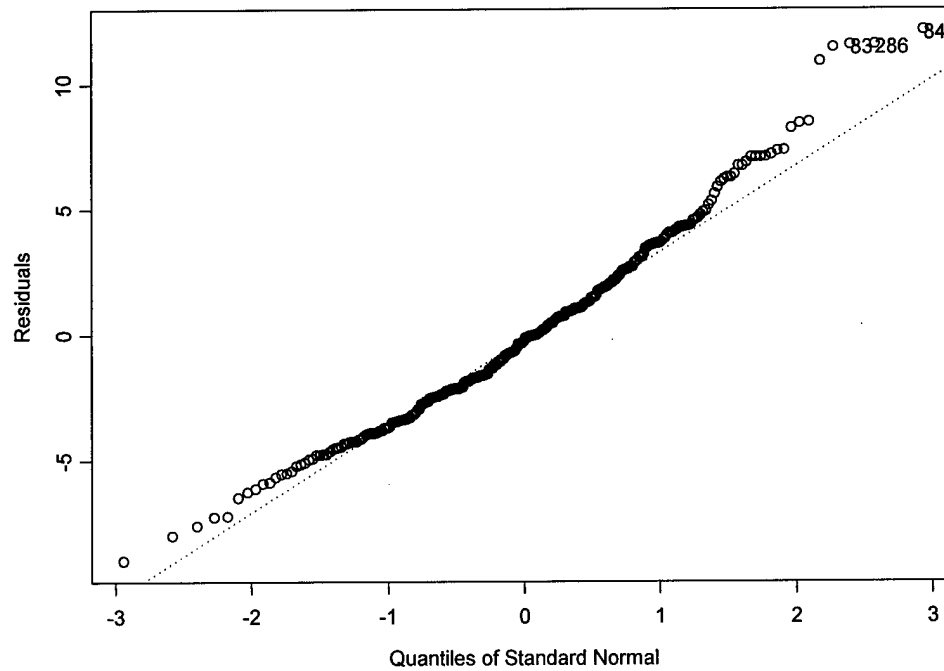


Figure B6: Normality Plot for Desert Land Type

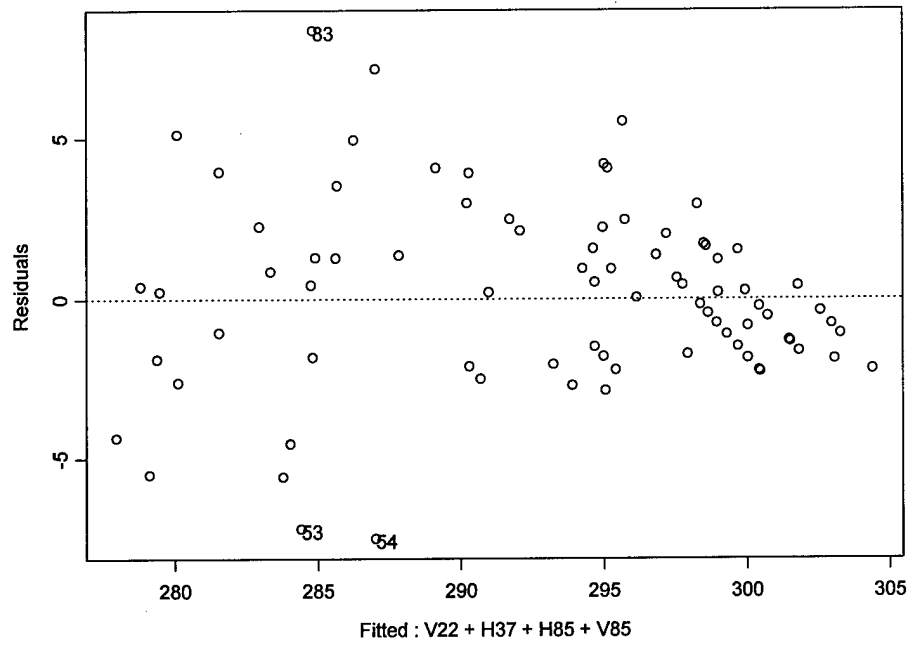


Figure B7: Residual Plot for Dense Vegetation Land Type

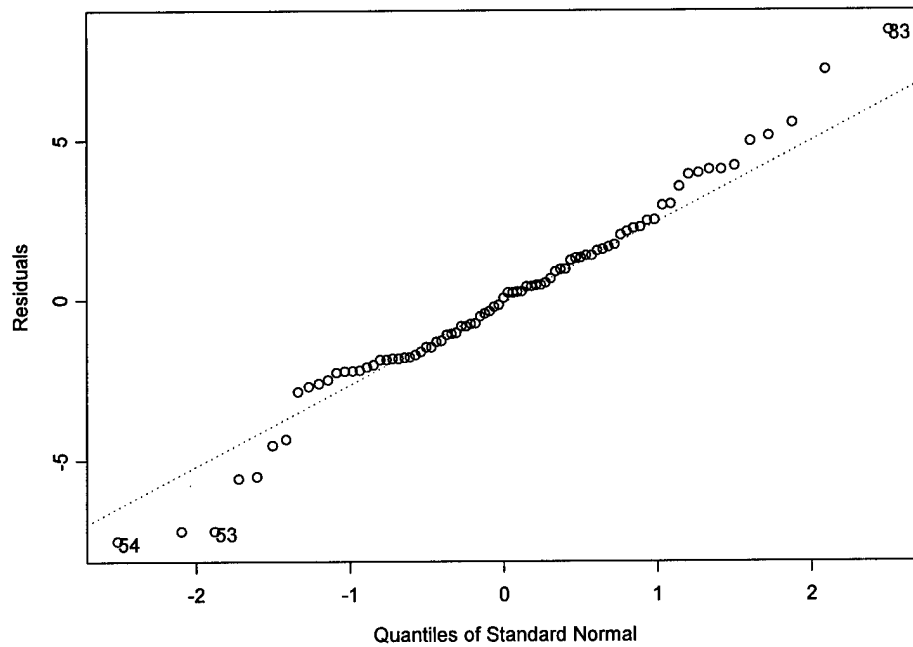


Figure B8: Normality Plot for Dense Vegetation Land Type

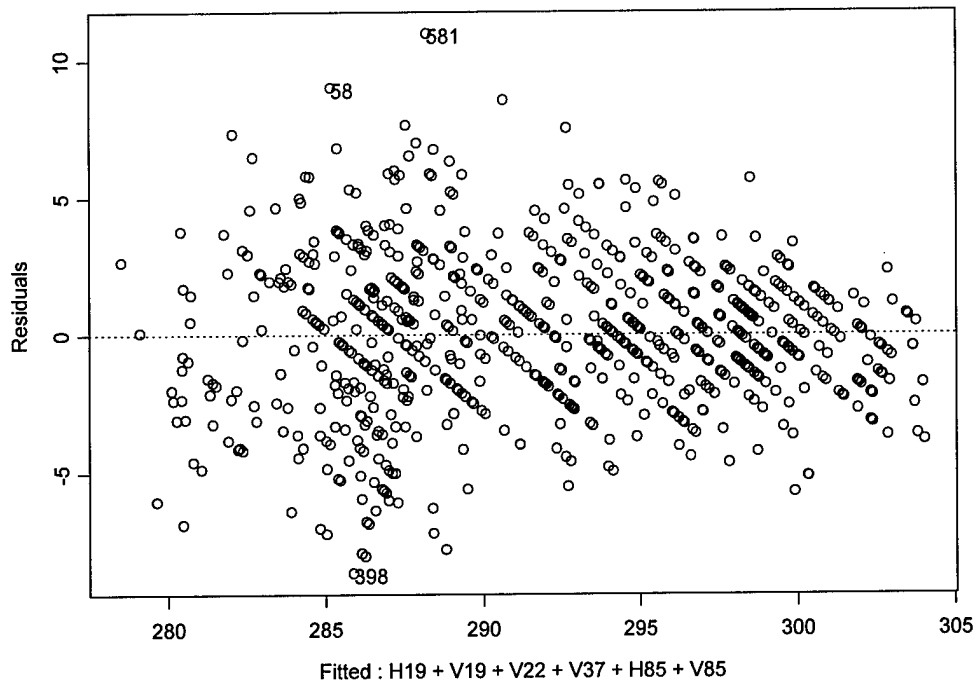


Figure B9: Residual Plot for Light Vegetation Land Type

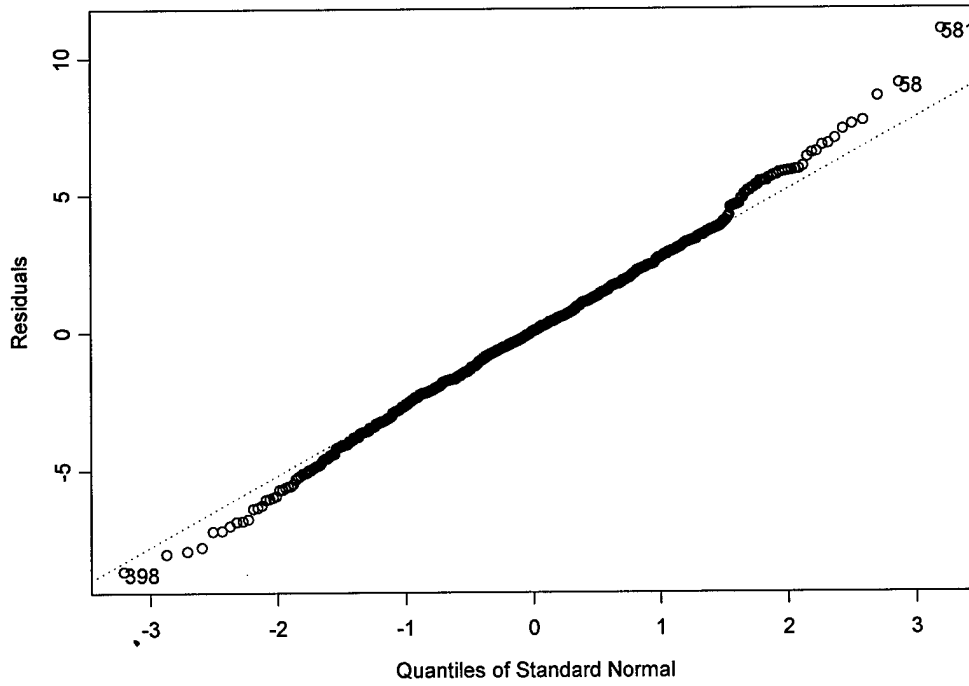


Figure B10: Normality Plot for Light Vegetation Land Type

Appendix C: CV Land Type Algorithms

If $(V22 - V19) \leq 4.0$ *and*
 $4.0 < (V19 + V37) / 2 \leq 9.8$ *and*
 $(V37 - V19) \geq -6.5$ *and*
 $-5.0 \leq (V85 - V37) < 0.5$ *and*
 $(H85 - H37) < 4.2$ *then*
land type = dry, arable soil

If $(V22 - V19) \leq 4.0$ *and*
 $4.0 < (V19 + V37) / 2 \leq 19.7$ *and*
 $(V37 - V19) \geq -6.5$ *and*
 $0.5 \leq (V85 - V37) < 4.0$ *and*
 $(V85 - H37) < 4.2$ *then*
land type = moist soil

If $(V22 - V19) \leq 4.0$ *and*
 $9.8 < (V19 + V37) / 2 \leq 19.7$ *and*
 $(V37 - V19) \geq 6.5$ *and*
 $(V85 - V37) < 0.5$ *and*
 $(H37 - H19) < -1.8$ *and*
 $(H85 - H37) < 6.0$ *then*
land type = semidesert

If $(V22 - V19) \leq 2.0$ *and*
 $(V19 + V37) / 2 \geq 19.7$ *and*
 $V19 > 268$ *and*
 $(H85 - H37) > -1.0$ *then*
land type = desert

If $(V22 - V19) \leq 4.0$ *and*
 $(V19 + V37)/2 \geq 6.4$ *and*
 $(V37 - V19) \geq -6.5$ *and*
 $(V85 - V37) < 0.5$ *and*
 $(H85 - H37) \geq 4.2$ *then*
land type = wet soil

If $(V22 - V19) \leq 4.0$ *and*
 $(V19 + V37)/2 \leq 1.9$ *and*
 $(V85 - V37) \geq -1.0$ *and*
 $(H85 - H37) < 4.5$ *and*
 $V19 > 262.0$ *then*
land type = dense vegetation

If $(V22 - V19) \leq 4.0$ *and*
 $(V19 + V37)/2 < 6.4$ *and*
 $(V85 - V37) \geq -1.0$ *and*
 $(H85 - H37) \geq 4.5$ *and*
 $(V37 - H37) > 257.0$ *then*
land type = mixed water and vegetation

If $(V22 - V19) \leq 4.0$ *and*
 $1.9 < (V19 + V37)/2 \leq 4.0$ *and*
 $(V85 - V37) \geq -1.0$ *and*
 $(H85 - H37) < 4.5$ *and*
 $V19 > 262.0$ *then*
land type = less dense vegetation

Bibliography

Betts, Alan K. and John H. Ball, "FIFE Surface Climate and Site-Average Dataset 1987-1989," Journal of the Atmospheric Sciences, Volume 55, 1091-1108, 1998

Cooper, Pat, "Air Force Launches DMSP Weather Satellite Built by Lockheed-Martin." WWWeb, <http://www.lmms.external.lmco.com/newsbureau/pressreleases/1997/9710.html> (25 Sep 98)

Comoglio, Ronald L., A Validation Study of the SSM/I Temperature Algorithm and Comparison with the CV Land Surface Temperatures. MS Thesis, AFIT/GM/ENP/97M-02. Graduate School of Engineering, Department of Engineering Physics, Air Force Institute of Technology (AU), Wright-Patterson AFB OH, 1997

Conner, Mark D., and Grant W. Petty, "Validation and Intercomparison of SSM/I Rain-Rate Retrieval Methods over the Continental United States," Journal of Applied Meteorology, Volume 37, 679-700, 1998

Coxwell, David, Captain, USAF. Satellite Weather Officer, 55th Space Weather Squadron, Schriever AFB CO. Personal Communication, 24 November 1998

Devore, Jay L., Probability and Statistics for Engineering and the Sciences. Belmont, CA: Wadsworth Publishing, 1995

Ferraro, Ralph R. et al., "A Screen Methodology for Passive Microwave Precipitation Retrieval Algorithms," Journal of the Atmospheric Sciences, Volume 55, 1583-1600, 1998

Fleagle, Robert G., and Joost A. Businger, An Introduction to Atmospheric Physics. New York: Academic Press, Inc., 1980

Harris, Charles H., Evaluation of Satellite Microwave Derived Surface Temperature Algorithms for the Period August 1996 to February 1997. MS Thesis, AFIT/GM/ENP/98M-04. Graduate School of Engineering, Department of Engineering Physics, Air Force Institute of Technology (AU), Wright-Patterson AFB OH, 1998

Hesser, William A., Global Evaluation of Special Sensor Microwave Imager Ocean Surface Wind Speed Retrieval Algorithms for the Period September 1991-April 1992. MS Thesis, Naval Postgraduate School, Monterey CA, 1995

Hollinger, J.P., SSM/I Project Summary Report, Naval Research Laboratory, Washington DC, 20 April 1983

- Hurrell, James W. and Kevin E. Trenberth, "Satellite versus Surface Estimates of Air Temperature since 1979," Journal of Climate, Volume 9, 2222-2232, 1996
- Kidd, C. et al., "The Advantages and Disadvantages of Statistically Derived-Empirically Calibrated Passive Microwave Algorithms for Rainfall Estimation," Journal of the Atmospheric Sciences, Volume 55, 1576-1582, 1998
- Kidder, Stanley Q. and Thomas H. Vonder Haar, Satellite Meteorology: an Introduction. New York: Academic Press, 1995
- Liu, Guosheng and Judith A. Curry, "An Investigation of the Relationship between Emission and Scattering Signals in SSM/I Data", Journal of the Atmospheric Sciences, Volume 55, 1628-1643, 1998
- McFarland, Marshall J. and others, "Land Parameter Algorithm Validation and Calibration," in DMSP Special Sensor Microwave Imager Calibration/Validation, Final Report, Volume II, Chapter 9, 40-64, 1991
- Neter, John, and William Wasserman, Applied Linear Statistical Models. Homewood, Illinois: Richard D. Irwin, Inc., 1974
- Neter, John, Wasserman, William, and Kutner, Michael H., Applied Linear Regression Models, 1st and 2nd edition. Homewood, Illinois: Richard D. Irwin, Inc., 1983 and 1989
- NGDC (National Geophysical Data Center), "The Defense Meteorological Satellite Program," WWWeb, www.ngdc.noaa.gov/dmsp/source/dmspdesc.html (10 Dec 98)
- NGDC (National Geophysical Data Center), "The SSM/I," WWWeb, www.ngdc.noaa.gov/dmsp/source/ssmi.html (10 Dec 98)
- Prata, A.J., "Land Surface Temperature Determination from Satellites," Advances in Space Research, Volume 14, 15-26, 1994
- Rees, W.G., Physical Principles of Remote Sensing. Cambridge, England: Cambridge University Press, 1990
- Ritchie, Adrian A. et al., "Critical Analyses of Data Differences between FNMOC and AFGWC Spawned SSM/I Datasets, Journal of the Atmospheric Sciences, Volume 55, 1601-1612, 1998
- Schmugge, T. J. and G.M. Schmidt, "Surface Temperature Observations from AVHRR in FIFE," Journal of the Atmospheric Sciences, Volume 55, 1239-1246, 1998
- Ulaby, Fawwaz T., et al. Microwave Remote Sensing: Active and Passive. 3 vols. Reading MA: Addison-Wesley Publishing Company, 1981,1982,1986

Wentz, Frank J. and Roy W. Spencer, "SSM/I Rain Retrievals within a Unified All-Weather Ocean Algorithm", Journal of the Atmospheric Sciences, Volume 55, 1613-1627, 1998

Vita

Captain Adair was born in Boston, Massachusetts on November 16, 1968. He was raised in Medford and Dracut, Massachusetts. He attended Dracut High School and graduated in 1986.

In September 1986, Captain Adair entered the Reserve Officer Training Corps (ROTC) at Boston University, Boston, Massachusetts. He graduated from Boston University's College of Liberal Arts in May 1990 with a Bachelor of Arts in Physics. He was commissioned a Second Lieutenant in the United States Air Force on May 23, 1990.

Captain Adair's first assignment was to the Air Force Institute of Technology's (AFIT) Basic Meteorology Program (BMP) at the Pennsylvania State University, University Park, Pennsylvania. He graduated Penn State in May of 1991 with a Bachelor of Science in Meteorology.

In June of 1991, Captain Adair was assigned to Detachment 4, 5th Weather Squadron, Fort Drum, New York, where he served as Officer in Charge of the Cadre Weather Team and Staff Weather Officer for the 10th Aviation Brigade, 10th Mountain Division (Light Infantry). Captain Adair was instrumental in procuring tactical equipment for the fledgling Aviation Brigade Weather team and was commended by the Division Commanding General for outstanding support during the Division's Battle Command Training Program (BCTP) Warfighter Exercise in April of 1992.

In January of 1993, Captain Adair was assigned as Weather Support Team Chief, European Forecast Unit (EFU), German Military Geophysical Office (GMGO), Traben-Trarbach, Germany. He supervised the production of routine and contingency forecast, advisory and warning products for the U.S. Air Force and U.S. Army, including aerodrome forecasts and long-range outlooks for operations in the former Yugoslavia.

In May of 1995, Captain Adair was assigned as Meteorological and Oceanographic (METOC) Staff Officer, U.S. European Command, Stuttgart, Germany. He served with distinction as Operations Staff Officer to the EUCOM Crisis Response Cell (CRC) during Operation DELIBERATE FORCE and as Executive Officer of the EUCOM Joint Operations Center (JOC) during Operation JOINT ENDEAVOR.

Captain Mark Adair arrived in August of 1997 to the Air Force Institute of Technology to pursue a Masters Degree in Meteorology. He has a follow on assignment as Meteorological Consultant to the Wargaming Technology and Assessment Branch, Air Force Research Laboratory (AFRL), Hanscom AFB, Massachusetts.

Permanent Address: 198 M Street
Boston MA 02127

REPORT DOCUMENTATION PAGE			Form Approved OMB No. 0704-0188	
Public reporting burden for this collection of information is estimated to average 1 hour per response, including the time for reviewing instructions, searching existing data sources, gathering and maintaining the data needed, and completing and reviewing the collection of information. Send comments regarding this burden estimate or any other aspect of this collection of information, including suggestions for reducing this burden, to Washington Headquarters Services, Directorate for Information Operations and Reports, 1215 Jefferson Davis Highway, Suite 1204, Arlington, VA 22202-4302, and to the Office of Management and Budget, Paperwork Reduction Project (0704-0188), Washington, DC 20503.				
1. AGENCY USE ONLY (Leave blank)		2. REPORT DATE 1 Mar 99	3. REPORT TYPE AND DATES COVERED Final	
4. TITLE AND SUBTITLE A Refinement and Cross-Validation of the Special Sensor Microwave Imager (SSM/I) Calibration-Validation (CV) Brightness Temperature Algorithm			5. FUNDING NUMBERS	
6. AUTHOR(S) Capt Mark R. Adair				
7. PERFORMING ORGANIZATION NAME(S) AND ADDRESS(ES) Maj Derrill T. Goldizen AFIT/ENP 2950 P Street Wright-Patterson AFB OH 45433-7765			8. PERFORMING ORGANIZATION REPORT NUMBER AFIT/GM/ENP/99M-01	
9. SPONSORING/MONITORING AGENCY NAME(S) AND ADDRESS(ES) Major Michael Farrar HQ AFWA/DNXM 106 Peacekeeper DR., Ste 2N3 Offutt AFB NE 68113-3505 Phone: (402) 294-4671			10. SPONSORING/MONITORING AGENCY REPORT NUMBER	
11. SUPPLEMENTARY NOTES				
12a. DISTRIBUTION AVAILABILITY STATEMENT Approved for public release; distribution unlimited			12b. DISTRIBUTION CODE	
13. ABSTRACT (Maximum 200 words) The Air Force Weather Agency (AFWA) currently uses an algorithm to calculate surface temperatures from microwave observations taken by the Special Sensor Microwave Imager (SSM/I) aboard the orbiting platforms of the Defense Meteorological Satellite Program (DMSP). This algorithm, called the Calibration-Validation (CV) algorithm, used multiple linear regression to calculate coefficients relating microwave brightness temperatures and land surface temperatures. Because the coefficients in this algorithm do not take into account the identity of the individual satellite, the question arose whether this assumption was valid. This thesis used multiple linear regression, stepwise linear regression, and qualitative regression on 3700 data sets from October of 1996 and September of 1997, including microwave brightness temperatures from three satellites. This data was analyzed to determine if satellite identity had a significant impact on CV regression coefficients. Analysis indicated that satellite identity does not have a significant impact on regression coefficients for five of the eight CV land types investigated. Analysis of two CV land types indicated data set identity had a significant impact, while there was insufficient data to determine the impact for one CV land type. In addition to the qualitative regression, stepwise linear regression was performed on five land type categories using combined data for all satellites. Regressed RMSEs ranged from 2.825 K to 3.743 K, while R squared values ranged from .7295 to .8613. Preliminary analysis indicated refinement of CV brightness temperature coefficients might yield better accuracy for the algorithm.				
14. SUBJECT TERMS SSM/I, DMSP, Passive Microwave Radiometry, Land Surface Temperatures, Remote Sensing			15. NUMBER OF PAGES 100	
			16. PRICE CODE	
17. SECURITY CLASSIFICATION OF REPORT Unclassified	18. SECURITY CLASSIFICATION OF THIS PAGE Unclassified	19. SECURITY CLASSIFICATION OF ABSTRACT Unclassified	20. LIMITATION OF ABSTRACT UL	